J. Fluid Mech. (2004), *vol.* 512, *pp.* 257–311.
DOI: 10.1017/S0022112004009929 Printed in the United Kingdom

Exact theory of unsteady separation for two-dimensional flows

By G. HALLER

Department of Mechanical Engineering, Massachusetts Institute of Technology,
77 Massachusetts Avenue, Rm 3-352, Cambridge, MA 02139, USA
ghaller@mit.edu

(Received 4 November 2002 and in revised form 26 March 2004)

We use a dynamical systems approach to extend Prandtl's steady separation criterion to two-dimensional unsteady flows with no-slip boundaries. Viewing separation profiles as non-hyperbolic unstable manifolds in the Lagrangian frame, we obtain explicit Eulerian formulae for the location of flow separation and reattachment on fixed and moving boundaries. We also derive high-order approximations for the unsteady separation profile in the vicinity of the boundary. Our criteria and formulae only use the derivatives of the velocity field along the boundary, and hence are of use in monitoring and controlling separation. In particular, we predict unsteady flow separation points and separation angles from distributed pressure and skin-friction measurements along the wall. As an example, we predict and verify separation points and separation profiles in variants of a two-dimensional oscillating separation-bubble flow.

1. Introduction

1.1. *Steady separation*

Prandtl (1904) showed that streamlines in a steady flow past a two-dimensional streamlined body separate from the boundary where the skin friction (or wall shear) vanishes and admits a negative gradient. Specifically, let $y = 0$ be the flat boundary of a steady incompressible velocity field $(u(x, y), v(x, y))$, and let τ_w denote the skin friction along the wall. Then steady separation takes place at a point $(p, 0)$ if

$$\left.\begin{aligned} \tau_w(p) &= \nu\rho\, u_y(p, 0) = 0, \\ \tau_w'(p) &= \nu\rho u_{xy}(p, 0) < 0, \end{aligned}\right\} \tag{1.1}$$

where ν is the kinematic viscosity and ρ is the density of the fluid. Although commonly thought otherwise, the steady separation conditions (1.1) are purely kinematic: they can be derived for any two-dimensional compressible velocity field that conserves mass (see, e.g. Shariff, Pulliam & Ottino 1991).

Prandtl's conditions give an Eulerian criterion for a Lagrangian phenomenon, the convergence and subsequent ejection of fluid particles from the vicinity of the boundary. This simple Lagrangian picture of separation is invoked in most introductory texts (see, e.g. Tritton 1988; Lugt 1995; Schlichting & Gersten 2000; Sobey 2000), although it is rarely noted in the research literature.

To illustrate the Lagrangian aspects of flow separation, figure 1 shows the motion of fluid particles in a separation-bubble model derived by Ghosh, Leonard & Wiggins (1998). Note how an initial upwelling, then a singular-looking tip, then a sharp

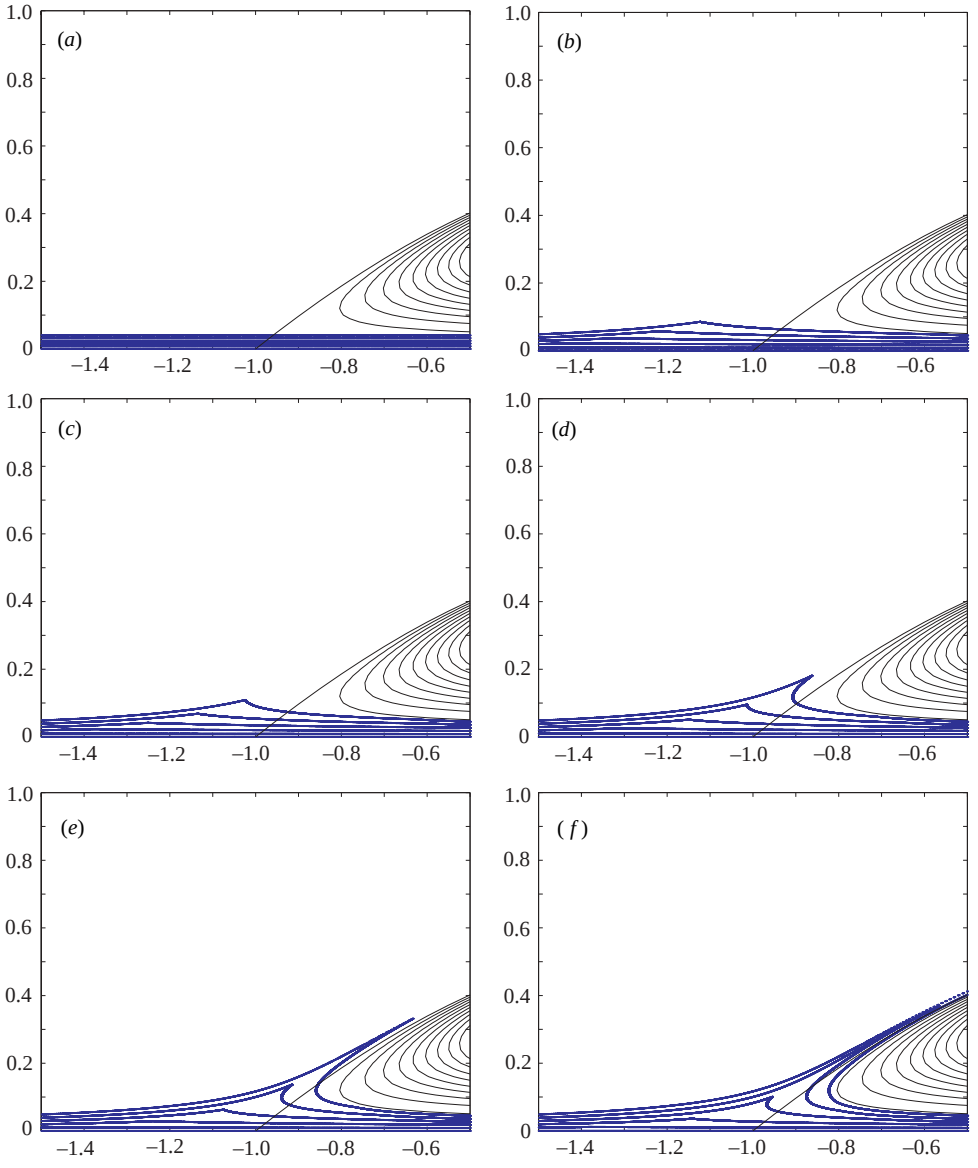

FIGURE 1. Separation evidenced by a layer of fluid particles in a steady separation bubble model (see § 9 for more information). Also shown are the streamlines inside the separation bubble.

material spike form in succession out of a set of material lines that initially align with the wall. Despite what is suggested by the initial upwelling and the tip, separation takes place at the point of attachment of a distinguished streamline, as predicted by (1.1). Accordingly, particles are attracted to, and ejected by, the distinguished streamline itself.

As the above example shows, steady flow separation appears as an instability in the Lagrangian frame. This instability is owing to the presence of a distinguished fixed point (the separation point) whose unstable manifold is the singular streamline described above. This unstable manifold acts as an attracting material line that

collects and transports particles away from the wall. The distinguished fixed point is degenerate owing to the no-slip boundary conditions, and hence its location and stability cannot be predicted from linearization. Prandtl's first condition in (1.1) gives a necessary condition for the existence of such a degenerate fixed point, while (1.1) as a whole gives a sufficient set of conditions for the existence of an unstable manifold.

1.2. *Prior work on unsteady separation*

For unsteady velocity fields, the Lagrangian and Eulerian descriptions of separation differ. On the Eulerian side, initial suggestions that unsteady flow separation also takes place at points of zero skin friction were dismissed by numerical simulations of boundary-layer separation by Rott (1956), Moore (1958) and Sears & Telionis (1971). Specifically, Sears & Telionis (1975) observed that vanishing wall shear 'does not denote separation in any meaningful sense in unsteady flow', and proposed a separation criterion that has become known as the Moore–Rott–Sears (MRS) principle.

According to the MRS principle, unsteady separation takes place at a point off the boundary where the wall-component of the shear vanishes and the local streamwise velocity equals the velocity of the moving separation structure. This postulate, however, requires the *a priori* knowledge of the separation speed, making the MRS principle difficult, if not impossible, to apply (Williams 1977; Van Dommelen 1981).

On the Lagrangian side, Van Dommelen (1981) and Van Dommelen & Shen (1982) initiated the numerical study of unsteady boundary-layer separation in Lagrangian coordinates. This approach has removed earlier computational difficulties seen in the Eulerian frame, and revealed the true Lagrangian signature of unsteady separation. As explained by Cowley, Van Dommelen & Lam (1990), this frame-independent signature is precisely the one shown in figure 1. The contraction of an infinitesimal fluid element in the streamwise direction is accompanied by a spiky expansion in the wall-normal direction.

Van Dommelen and coworkers attribute the material spike to the formation of a singularity in the boundary-layer equations, and define the unsteady separation point as the location of the singularity. A number of separation studies have since confirmed the advantages of Lagrangian coordinates (see, e.g. Peridier 1995; Cassel, Smith & Walker 1996; Degani, Walker & Smith 1998), and formal asymptotic expansions are available for Van Dommelen's singularity in the boundary-layer equations (Cowley 1983; Van Dommelen & Cowley 1990). Analytic results show, however, that separation in the boundary-layer equations has no direct connection with velocity singularities (Liu & Wan 1985).

Despite computational advances on boundary-layer separation, a theoretically sound description has been missing for general unsteady flow separation, a phenomenon that is equally common for high and low Reynolds numbers. As Sears & Telionis (1975) point out, we would ideally need an unsteady separation definition that does not depend on our ability to solve the boundary-layer equations accurately. Secondly, as suggested by Cowley *et al.* (1990), an ideal separation definition should be independent of the coordinate system selected. Thirdly, as argued by Wu *et al.* (2000), the growing interest in active flow control calls for a separation criterion that uses quantities measured or computed along the boundary.

The Lagrangian definition of steady separation (reviewed in connection with figure 1) has the above three ingredients, and hence is an ideal starting point for a rigorous unsteady separation theory. Such a theory was first proposed by

Shariff *et al.* (1991) for two-dimensional incompressible time-periodic flows. Shariff *et al.* defined the separation point as a fixed point with an unstable manifold for the Poincaré map associated with the periodic flow. Using this Lagrangian definition, they showed that unsteady separation points are located at boundary points where the time-average of the skin friction vanishes. This remarkable result, however, is based on an assertion on the Poincaré map that has remained unverified ever since.

Realizing the above shortcoming, Yuster & Hackborn (1997) re-derived the zero-mean-friction principle for near-steady time-periodic incompressible flows in a mathematically rigorous way; Hackborn, Ulucakli & Yuster (1997) verified the result experimentally. The validity of the zero-mean-skin friction principle for general time-periodic flows, however, has remained an open question. As a notable contribution, Yuster & Hackborn (1997) showed that the principle fails for compressible time-periodic flows.

In summary, the only available rigorous unsteady separation criterion has been the zero-mean-friction principle, which applies to time-periodic incompressible flows that are close to a steady limit. No results have been derived for compressible flows, or for flows with general time dependence. In addition, no rigorous theory has been proposed for moving separation, which cannot be explained by classical unstable manifolds (cf. § 8).

1.3. *Results on fixed separation*

In this paper, we extend the Lagrangian view of separation from steady flows to compressible unsteady flows with general time dependence. Specifically, we define fixed unsteady flow separation as a material instability induced by an unstable manifold of a distinguished boundary point. In this general context, the unstable manifold is a time-dependent material line that shrinks to the separation point in backward time. In forward time, the unstable manifold attracts and ejects particles from a vicinity of the boundary.

Using the above Lagrangian definition, we derive mathematically exact Eulerian criteria that locate time-dependent unstable manifolds emanating from the wall. Because of the degeneracy (non-hyperbolicity) of fixed points on a no-slip wall, classical dynamical systems methods for locating their unstable manifolds fail to apply. Equally inapplicable are the Poincaré-map arguments of Shariff *et al.* (1991) and Yuster & Hackborn (1997) because of the general time-dependence we allow for. To overcome these limitations of classical invariant manifold theory, we develop a novel nonlinear technique that renders both the location and the shape of unstable manifolds or *separation profiles*.

We show that *fixed* (i.e. non-moving) *separation* takes place where the weighted backward-time average of the skin friction remains uniformly bounded. The weight function in this average is just the squared reciprocal of the fluid density. We also clarify the meaning of *effective separation points* at which the weighted finite-time mean of the skin friction vanishes. These points turn out to converge to fixed separation points provided that an unsteady version of Prandtl's second separation condition (cf. (1.1)) holds.

When applied to simple flows, our criteria agree with prior exact separation criteria for such flows. Specifically, for steady flows, our general criteria coincide with those of Prandtl (1904) and Lighthill (1963). When applied to incompressible time-periodic flows, our results agree with those of Shariff *et al.* (1991) and Yuster & Hackborn (1997). Finally, when translated into the Lagrangian frame, our separation criterion agrees with the second criterion of Van Dommelen (1981) for boundary-layer

separation. Most importantly, however, our kinematic theory predicts unsteady flow separation in general velocity fields that are inaccessible to previous theories.

1.4. *Results on moving separation*

By *moving separation* we mean separation where the separation point may move, disappear and reappear. In such cases, classical invariant manifold theory turns out to be inapplicable; we need to use finite-time unstable manifolds (Haller 2000, 2001) to describe moving separation profiles. Finite-time unstable manifolds are inherently non-unique, and so are moving separation profiles. The distance between two separation profiles, however, tends to zero as their time of existence increases (Haller 2000).

We present two approaches to moving separation: a heuristic and a rigorous one. The first approach assumes that the backward-time integral of the skin friction has a well-defined mean component, or equivalently, that a well-defined mean separation profile exists in the Lagrangian frame. This assumption leads to a heuristic *necessary criterion* that identifies moving separation as a bifurcation in the mean evolution of wall-bound material lines.

When applied to analytic flow models, the heuristic criterion yields explicit expressions for the location and shape of the moving separation profile. When applied to numerical or experimental data, the criterion gives separation profiles that converge to the moving profile as more and more past velocity data is processed in the calculation.

Our second method for locating moving separation, a *sufficient criterion*, is based on a rigorous analytic construction of finite-time unstable manifolds near effective separation points. Effective separation points depend sensitively on the time scale over which they are computed, but we find the time scale for which they closely approximate a nearby moving separation point. This time scale results from a general analytic estimate that may be further strengthened for particular classes of flows.

With the exception of quasi-periodic and periodic flows, most unsteady flows produce moving separation, and hence should be analysed by the above two criteria. If the separation happens to be fixed, the heuristic necessary criterion produces moving separation points that converge to the fixed separation point after initial transients. By contrast, our sufficient criterion yields separation points that are close to the fixed separation from the start, but this closeness may not improve further in time.

As we illustrate in examples, our moving separation criteria perform reliably under both regular and stochastic time dependence, suggesting that the separation theory described here is equally applicable to laminar and turbulent flows.

1.5. *Organization of the paper*

We derive necessary conditions for fixed compressible separation in § 2, and give a quadratic approximation for a general compressible separation profile. Section 2 also contains equivalent Lagrangian and density-independent formulations of our criteria, as well as the treatment of moving and non-smooth boundaries. We show how the theory simplifies for incompressible flows in § 3, and exploit this simplification to derive a quartic-order approximation for incompressible separation profiles.

In § 4, we give a kinetic version of our separation criteria for Navier–Stokes flows, and, in § 5, we formulate sufficient conditions for sharp unsteady separation. Section 6 shows how our fixed separation criteria simplify to steady time-periodic and quasi-periodic flows. Fixed unsteady reattachment is discussed in § 7, and moving unsteady separation and reattachment are treated in § 8. We illustrate our separation criteria on different versions of a kinematic flow model in § 9, and present our conclusions in § 10.

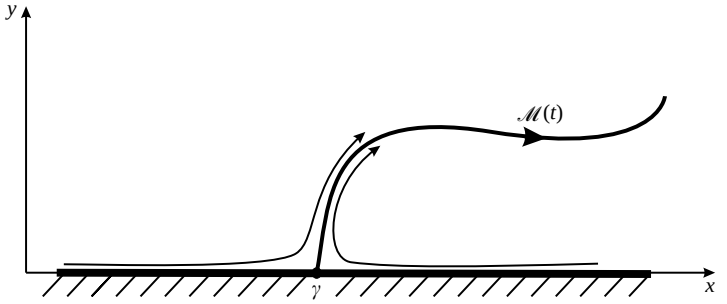

FIGURE 2. Unsteady separation profile viewed as a time-dependent material line that guides particles away from the wall.

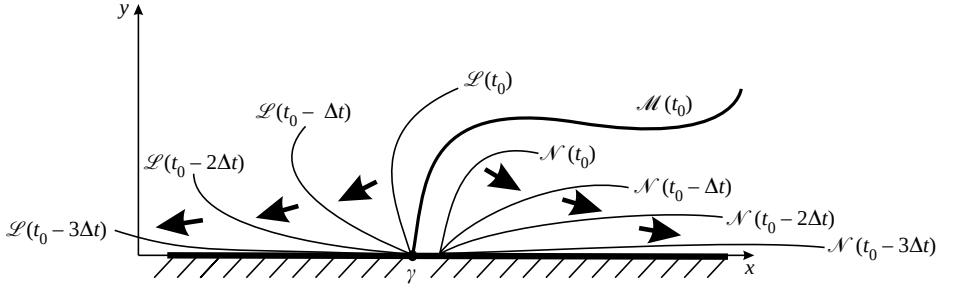

FIGURE 3. Behaviour of typical material lines in backward time near a separation profile $\mathscr{M}(t)$. The line $\mathscr{N}(t)$ attaches to the wall away from the separation point. The line $\mathscr{L}(t)$ attaches to the wall at the separation point, but does not coincide with the separation profile.

2. Fixed unsteady separation

2.1. *Set-up*

Consider a two-dimensional velocity field $\boldsymbol{v}(x, y, t) = (u(x, y, t), v(x, y, t))$, with the induced fluid particle motion satisfying

$$\dot{x} = u(x, y, t), \qquad \dot{y} = v(x, y, t). \tag{2.1}$$

Assume further that a boundary is present in the flow at $y = 0$ with the no-slip boundary conditions

$$u(x, 0, t) = v(x, 0, t) = 0. \tag{2.2}$$

We seek a time-dependent material line $\mathscr{M}(t)$ – the *separation profile* – that collects and ejects fluid particles from a vicinity of the boundary (figure 2). As a material line, $\mathscr{M}(t)$ is anchored to the same boundary point γ for all times owing to the no-slip boundary conditions. In dynamical systems terms, $\mathscr{M}(t)$ is an unstable manifold for a fixed point of the $y = 0$ boundary.

By *fixed unsteady flow separation* we mean the type of separation induced by $\mathscr{M}(t)$. Specifically, fluid particles are ejected along $\mathscr{M}(t)$ in the form of a thin spike from the vicinity of the boundary into the main stream. The spike aligns with $\mathscr{M}(t)$, whose shape changes in time, but whose point of attachment remains fixed. As shown in figure 3, generic material lines emanating from the boundary converge to the boundary as $t \to -\infty$. Fixed unsteady separation profiles, such as $\mathscr{M}(t)$, are exceptions to this rule, and this property renders them explicitly computable, as we shall see below.

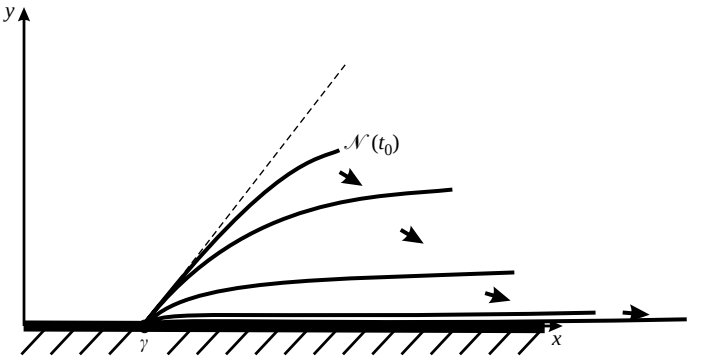

FIGURE 4. Time history of a hypothetical material line $\mathscr{N}(t_0)$ whose first derivative at the wall remains bounded, but whose curvature grows unbounded in backward time. The graph of the function $x = y - ty^2$ is an example of a time-dependent curve of the type $\mathscr{N}(t)$.

To exclude degenerate or unphysical cases of separation, we shall only consider separation profiles with the following properties:

1. The separation profile is *unique*: no other separation profiles emerges from the same boundary point.
2. The separation profile is *transverse*, i.e. $\mathscr{M}(t)$ is not tangent to the boundary.
3. The separation profile is *regular* up to nth order: $\mathscr{M}(t)$ admits n derivatives ($n \geqslant 1$) that remain uniformly bounded at $y = 0$ for all times.

Properties 1 and 2 express plausible physical features of separation. Property 3 is to exclude separation profiles that enclose a bounded angle with the boundary, but still end up approaching the boundary owing to unbounded growth in their higher derivatives (cf. figure 4). We shall call a separation profile with n uniformly bounded derivatives at the wall an nth-*order separation profile*.

By its definition, fixed separation is present for all times in the flow, and hence transient phenomena – such as the creation, destruction and movement of separation points – do not arise in its study. Fixed separation is, therefore, relevant for flows with recurrent time dependence, such as time-periodic or quasi-periodic flows (see § 6 for examples). In such flows, fixed separation may also take place around general curved boundaries (cf. § 2.9). For flows with non-recurrent time dependence, *moving separation* will be the relevant concept (cf. § 8).

2.2. *Assumptions*

We assume that no sinks or sources are present at separation, and hence the continuity equation

$$\rho_t + \nabla \cdot (\rho \boldsymbol{v}) = 0 \tag{2.3}$$

holds for the density $\rho(x, y, t)$ in the neighbourhood of a separation point $(x, y) = (\gamma, 0)$. Because of the no-slip boundary conditions at $y = 0$, the continuity equation simplifies to

$$\rho_t(x, 0, t) + \rho(x, 0, t) v_y(x, 0, t) = 0 \tag{2.4}$$

at boundary points, leading to the density relation

$$\rho(x, 0, t) = \rho(x, 0, t_0) \exp\left(- \int_{t_0}^{t} v_y(x, 0, s)\, \mathrm{d}s \right). \tag{2.5}$$

Differentiation of (2.5) with respect to x gives the wall-tangential density gradient evolution

$$\rho_x(x,0,t) = \rho_x(x,0,t_0)\exp\left(-\int_{t_0}^{t} v_y(x,0,s)\,\mathrm{d}s\right) - \rho(x,0,t_0)\exp\left(-\int_{t_0}^{t} v_y(x,0,s)\,\mathrm{d}s\right)\int_{t_0}^{t} v_{xy}(x,0,s)\,\mathrm{d}s. \quad (2.6)$$

The density of the fluid should remain bounded from below and from above for all times along the boundary. Thus, we may assume that for appropriate $\rho_2 > \rho_1 > 0$ and for all t,

$$0 < \rho_1 \leqslant \rho(x,0,t) \leqslant \rho_2 < \infty \quad (2.7)$$

holds along the boundary region of interest.

Next we assume that the tangential density gradient along the boundary remains uniformly bounded near the separation point for all times. In view of (2.5), (2.6) and (2.7), this second assumption is equivalent to

$$\left|\int_{t_0}^{t} v_{xy}(x,0,s)\,\mathrm{d}s\right| \leqslant K_1 < \infty, \quad (2.8)$$

for an appropriate constant K_1, for any time t, and for all x values near γ.

Assumptions (2.7) and (2.8) hold automatically for incompressible flows, because for such flows,

$$v_y(x,0,t) \equiv 0, \qquad v_{xy}(x,0,t) \equiv 0. \quad (2.9)$$

2.3. *Equation for the separation profile*

Using the no-slip boundary condition, we rewrite (2.1) as

$$\dot{x} = yA(x,y,t), \qquad \dot{y} = yB(x,y,t), \quad (2.10)$$

where

$$A(x,y,t) = \int_0^1 u_y(x,sy,t)\,\mathrm{d}s, \qquad B(x,y,t) = \int_0^1 v_y(x,sy,t)\,\mathrm{d}s. \quad (2.11)$$

Next we recall that fixed unsteady separation occurs if a boundary point $\boldsymbol{p} = (\gamma, 0)$ admits an unstable manifold $\mathscr{M}(t)$ that is not tangent to the boundary. In that case, the unstable manifold is locally represented by a time-dependent graph

$$x = \gamma + yF(y,t), \quad (2.12)$$

as shown in figure 5.

Substitution of (2.12) into (2.10) gives

$$y[B(\gamma + yF, y, t)F + yF_yB(\gamma + yF, y, t) + F_t - A(\gamma + yF, y, t)] = 0. \quad (2.13)$$

For continuously differentiable separation profiles, the bracketed expression in (2.13) must be zero for all $y \geqslant 0$. (It is certainly zero for $y > 0$, and it cannot take any other value but zero at $y = 0$ by continuity.) As a result, (2.14) implies that the separation profile must satisfy the partial differential equation

$$F_t = A(\gamma + yF, y, t) - B(\gamma + yF, y, t)F - yF_yB(\gamma + yF, y, t). \quad (2.14)$$

We shall use this separation equation to deduce necessary criteria for separation, and to devise approximations to the separation profile. Such approximations will be

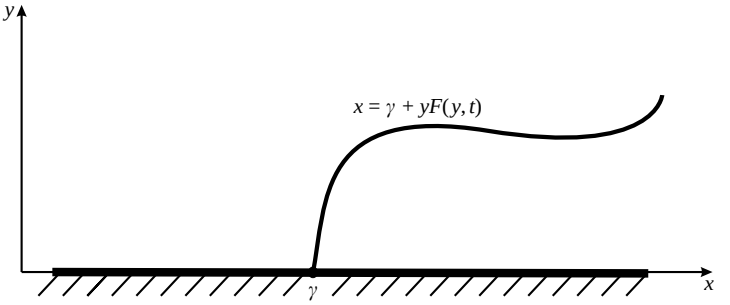

FIGURE 5. Near the wall, the separation profile can be viewed as a graph over the y variable, because we have assumed non-tangential separation.

obtained from a series expansion

$$F(y,t) = f_0(t) + yf_1(t) + \tfrac{1}{2}y^2 f_2(t) + \ldots, \tag{2.15}$$

where

$$f_0(t) = F(0,t), \qquad f_1(t) = F_y(0,t), \qquad f_2(t) = F_{yy}(0,t). \tag{2.16}$$

2.4. *Necessary conditions for separation*

To simplify our notation, we let

$$a(t) = A(\gamma,0,t), \qquad b(t) = B(\gamma,0,t), \qquad \rho(t) = \rho(\gamma,0,t), \tag{2.17}$$

where $(\gamma,0)$ is the separation point we wish to characterize. We also rewrite (2.5) in our new notation as

$$\rho(t) = \rho(t_0)\exp\left(-\int_{t_0}^{t} b(s)\,\mathrm{d}s\right). \tag{2.18}$$

Setting $y = 0$ in the separation equation (2.14), we obtain the linear differential equation

$$\dot{f}_0(t) = -b(t)f_0(t) + a(t). \tag{2.19}$$

The general solution of this equation is

$$f_0(t) = f_0(t_0)\frac{\rho(t)}{\rho(t_0)} + \rho(t)\int_{t_0}^{t}\frac{a(\tau)}{\rho(\tau)}\,\mathrm{d}\tau, \tag{2.20}$$

where we used (2.18).

Recall that $f_0(t)$ is the tangent of the angle that the separation profile encloses with the wall-normal direction at $\xi = y = 0$. Fixed separation takes place at $x = \gamma$, if $f_0(t)$ remains bounded in backward time (cf. figure 3). By assumption (2.7), the first term on the right-hand side of (2.20) and the $\rho(t)$ factor in the second term are both bounded in backward time. Therefore, a necessary condition for separation is the boundedness of the integral of the second term in (2.20), which we express in the form

$$\limsup_{t\to-\infty}\left|\int_{t_0}^{t}\frac{u_y(\gamma,0,\tau)}{\rho(\gamma,0,\tau)}\,\mathrm{d}\tau\right| < \infty. \tag{2.21}$$

This criterion is an extension of Prandtl's first condition for steady separation, as we show in § 6.1. Notice that γ does not depend on t_0 in (2.21), because if the integral in (2.21) is bounded for a given t_0, then it will also be bounded for any other $\bar{t}_0$ (say, with $\bar{t}_0 > t_0$) by the boundedness of the integrand over the finite interval $[t_0, \bar{t}_0]$.

Just as Prandtl's first condition, (2.21) is also satisfied at any point of a fluid at rest, which shows the need for a second condition to describe separation. A second necessary condition turns out to be

$$\int_{t_0}^{-\infty} \left[\frac{1}{\rho(\tau)}(u_{xy}(\gamma,0,\tau) - v_{yy}(\gamma,0,\tau)) - 2v_{xy}(\gamma,0,\tau) \int_{t_0}^{\tau} \frac{u_y(\gamma,0,s)}{\rho(\gamma,0,s)}\,\mathrm{d}s \right] \mathrm{d}\tau = \infty, \tag{2.22}$$

as we show in Appendix A. This condition ensures that all material lines emanating from boundary points near γ converge to the wall in backward time, a feature that flows at rest do not possess. As we show in § 6.1, condition (2.22) simplifies to Prandtl's second separation condition when applied to steady flows.

2.5. *Effective separation points*

The theoretical necessary condition (2.21) can be expressed in a form more suitable for computations. To derive this equivalent form, we again recall that material lines emanating from any boundary point near $(\gamma, 0)$ align with the boundary as $t \to -\infty$. By formula (2.20), this asymptotic alignment in backward time is only possible if, for all small enough $|x - \gamma|$,

$$\int_{t_0}^{-\infty} \frac{u_y(x,0,\tau)}{\rho(x,0,\tau)}\,\mathrm{d}\tau = \begin{cases} +\infty & \text{if } x > \gamma, \\ -\infty & \text{if } x < \gamma. \end{cases} \tag{2.23}$$

Consequently, for any large constant $C > 0$ and for any small $\delta > 0$, we can select $t \ll t_0$ such that

$$\int_{t_0}^{t} \frac{u_y(x,0,\tau)}{\rho(x,0,\tau)}\,\mathrm{d}\tau \begin{cases} > C & \text{if } x = \gamma + \delta, \\ < -C & \text{if } x = \gamma - \delta. \end{cases} \tag{2.24}$$

Thus, not only is the backward integral of u_y/ρ bounded at separation, but it also admits a sign change arbitrarily close to the separation point for large enough $|t - t_0|$.

Because the integral

$$i_t(x) = \int_{t_0}^{t} \frac{u_y(x,0,\tau)}{\rho(x,0,\tau)}\,\mathrm{d}\tau \tag{2.25}$$

is a continuous function of x for any finite t, we conclude from (2.24) that $i_t(x)$ must admit at least one zero that approaches γ as t approaches $-\infty$. As a result, defining the *effective separation point* $\gamma_{eff}(t, t_0)$ via the formula

$$\int_{t_0}^{t} \frac{u_y(\gamma_{eff},0,\tau)}{\rho(\gamma_{eff},0,\tau)}\,\mathrm{d}\tau = 0, \tag{2.26}$$

we obtain

$$\gamma = \lim_{t \to -\infty} \gamma_{eff}(t, t_0), \tag{2.27}$$

as shown in figure 6.

Equations (2.26) and (2.27) give a practical algorithm for computing fixed unsteady separation points at time t_0 from velocity data. For a past time t with $|t - t_0|$ large enough, we compute the integral in $i_t(x)$ along the wall and find the effective separation point $\gamma_{eff}(t, t_0)$. By (2.27), this effective separation point will converge to the real separation point γ as $t \to -\infty$.

Three remarks are in order. (i) Fixed separation points of time-periodic or time-quasi-periodic flows are exactly computable from finite-time velocity data without the use of effective separation points (cf. § 6). (ii) The effective separation point $\gamma_{eff}(t, t_0)$

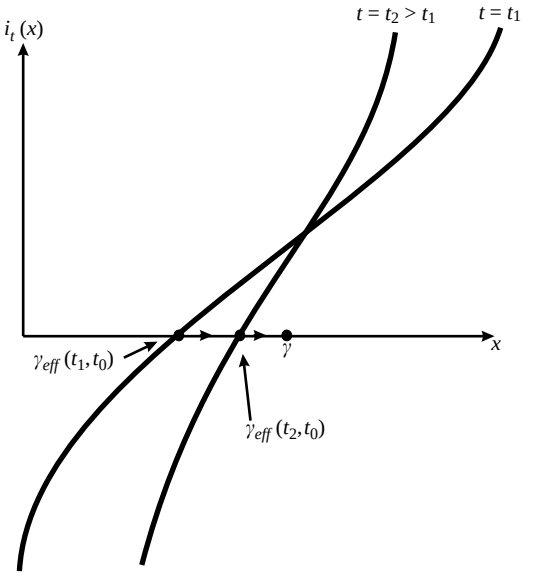

FIGURE 6. The convergence of the effective separation point to the actual separation point.

is a good approximation for the true separation point if we select $t = t_0 - T_m(t_0)$, where T_m will be defined in our discussion on moving separation (cf. § 8). (iii) Taking the limit $t \to -\infty$ in our formulae does not require solving for the velocity field in backward time; it requires computing longer and longer backward-time averages from the available velocity data as the current time t_0 progresses.

2.6. *Separation angle and curvature*

To obtain an expression for the angle of fixed unsteady separation, we first differentiate (2.14) with respect to y and set $y = 0$ to obtain the equation

$$\dot{f}_1 = a_x f_0 + a_y - b_x f_0^2 - b_y f_0 - 2bf_1. \tag{2.28}$$

Our notation here is consistent with that of the previous sections; for instance, we have $a_x(t) = A_x(\gamma, 0, t)$ and $f_1(t) = F_y(0, t)$.

Using the density formula (2.18), we write the solution of the above linear o.d.e. in the form

$$f_1(t) = f_1(t_0)\frac{\rho^2(t)}{\rho^2(t_0)} + \int_{t_0}^{t} \frac{\rho^2(t)}{\rho^2(\tau)}\left[a_y(\tau) + (a_x(\tau) - b_y(\tau))f_0(\tau) - b_x(\tau)f_0^2(\tau)\right] \mathrm{d}\tau. \tag{2.29}$$

For a second-order separation profile (i.e. for a profile of bounded curvature), the above solution must be bounded as $t \to -\infty$. As we show in Appendix A, this boundedness requirement leads to the following formula for the slope of the separation profile at $t = t_0$:

$$f_0(t_0) = \lim_{t \to -\infty} \frac{\rho(t_0)\displaystyle\int_{t_0}^{t} \left[\frac{b_y(\tau) - a_x(\tau)}{\rho(\tau)} \int_{t_0}^{\tau} \frac{a(s)}{\rho(s)}\,\mathrm{d}s + b_x(\tau)\left(\int_{t_0}^{\tau} \frac{a(s)}{\rho(s)}\,\mathrm{d}s\right)^2 - \frac{a_y(\tau)}{\rho^2(\tau)}\right]\mathrm{d}\tau}{\displaystyle\int_{t_0}^{t} \left[\frac{a_x(\tau) - b_y(\tau)}{\rho(\tau)} - 2b_x(\tau)\int_{t_0}^{\tau} \frac{a(s)}{\rho(s)}\,\mathrm{d}s\right]\mathrm{d}\tau}. \tag{2.30}$$

We recall that $f_0(t_0)$ gives the separation slope measured relative to the wall-normal direction at time $t = t_0$. Therefore, the angle of separation at $(\gamma, 0)$ is $\alpha(t_0) = \tan^{-1}(1/f_0(t_0))$ when measured from the boundary.

To obtain the next coefficient in the expansion (2.15) for the separation profile, we differentiate (2.14) twice with respect to y and set $y = 0$ to obtain

$$\begin{aligned}\dot{f}_2 = {} & a_{yy} + (2a_{xy} - b_{yy})f_0 + (a_{xx} - 2b_{xy})f_0^2 - b_{xx}f_0^3 \\ & + 2(a_x - 2b_y)f_1 - 6b_x f_0 f_1 - 3bf_2,\end{aligned} \tag{2.31}$$

an o.d.e. for the function $f_2(t)$. The solution of this equation is

$$\begin{aligned}f_2(t) = {} & f_2(t_0)\frac{\rho^3(t)}{\rho^3(t_0)} + \rho^3(t)\int_{t_0}^{t} \frac{a_{yy}(\tau) + f_0(\tau)(2a_{xy}(\tau) - b_{yy}(\tau))}{\rho^3(\tau)}\,\mathrm{d}\tau \\ & + \rho^3(t)\int_{t_0}^{t} f_0^2(\tau)\frac{a_{xx}(\tau) - 2b_{xy}(\tau) - b_{xx}(\tau)f_0(\tau)}{\rho^3(\tau)}\,\mathrm{d}\tau \\ & + 2\rho^3(t)\int_{t_0}^{t} f_1(\tau)\frac{a_x(\tau) - 2b_y(\tau) - 3b_x(\tau)f_0(\tau)}{\rho^3(\tau)}\,\mathrm{d}\tau.\end{aligned} \tag{2.32}$$

Again, the right-hand side of (2.32) should be bounded for all $t \leqslant t_0$ if $\xi = yF(y, t)$ is the graph of a third-order separation profile. Since the first term on the right-hand side is bounded by assumption (2.7), the sum of the remaining three terms must be bounded for all $t \leqslant t_0$. Repeating the arguments leading to (11.7) and (11.11) in Appendix A, then substituting (2.29) for $f(\tau)$ finally leads to

$$f_1(t_0) = -\lim_{t\to-\infty} \frac{\rho^2(t_0)\displaystyle\int_{t_0}^{t} [R(\tau) + S(\tau) + T(\tau)U(\tau)]\,\mathrm{d}\tau}{\displaystyle\int_{t_0}^{t} \rho^2(\tau)T(\tau)\,\mathrm{d}\tau}, \tag{2.33}$$

with

$$\left.\begin{aligned}R(\tau) &= \frac{a_{yy}(\tau) + f_0(\tau)(2a_{xy}(\tau) - b_{yy}(\tau))}{\rho^3(\tau)}, \\ S(\tau) &= f_0^2(\tau)\frac{a_{xx}(\tau) - 2b_{xy}(\tau) - b_{xx}(\tau)f_0(\tau)}{\rho^3(\tau)}, \\ T(\tau) &= 2\frac{a_x(\tau) - 2b_y(\tau) - 3b_x(\tau)f_0(\tau)}{\rho^3(\tau)}, \\ U(\tau) &= \int_{t_0}^{\tau} \frac{\rho^2(\tau)}{\rho^2(s)}\left[a_y(s) + (a_x(s) - b_y(s))f_0(s) - b_x(s)f_0^2(s)\right]\mathrm{d}s.\end{aligned}\right\} \tag{2.34}$$

Similar expressions can be derived for higher-order derivatives of $F(y, t)$ in a recursive fashion by further differentiating the separation equation (3.8) with respect to y at $y = 0$. Although these expressions are lengthy for general compressible flows, they become significantly simpler for incompressible flows (see § 3).

2.7. *Density-independent formulation*

Using the density relation (2.5), we can express the density in terms of the integral of $v_y(\gamma, 0, t)$, and obtain a density-independent formulation of our fixed separation

theory. In this formulation, assumptions (2.7) and (2.8) are expressed as

$$\left|\int_{t_0}^{t} v_y(x,0,s)\,\mathrm{d}s\right| \leqslant K_0 < \infty, \qquad \left|\int_{t_0}^{t} v_{xy}(x,0,\tau)\,\mathrm{d}\tau\right| \leqslant K_1 < \infty, \tag{2.35}$$

and the separation criteria (2.21) and (2.22) are replaced by

$$\limsup_{t\to-\infty}\left|\int_{t_0}^{t}\exp\left(\int_{t_0}^{\tau} v_y(\gamma,0,s)\,\mathrm{d}s\right)u_y(\gamma,0,\tau)\,\mathrm{d}\tau\right| < \infty \tag{2.36}$$

and

$$\int_{t_0}^{-\infty}\left[\exp\left(\int_{t_0}^{\tau} v_y(\gamma,0,s)\,\mathrm{d}s\right)(u_{xy}(\gamma,0,\tau)-v_{yy}(\gamma,0,\tau))\right.$$
$$\left.-2v_{xy}(\gamma,0,\tau)\left(\int_{t_0}^{\tau}\exp\left(\int_{t_0}^{s} v_y(\gamma,0,s)\,\mathrm{d}s\right)u_y(\gamma,0,s)\,\mathrm{d}s\right)\mathrm{d}\tau\right] = \infty. \tag{2.37}$$

Similarly, effective separation points are defined by the formula

$$\int_{t_0}^{t}\exp\left(\int_{t_0}^{\tau} v_y(\gamma_{eff},0,s)\,\mathrm{d}s\right)u_y(\gamma_{eff},0,\tau)\,\mathrm{d}\tau = 0. \tag{2.38}$$

The separation slope and curvature, as well as higher-order derivatives of the separation profile can all be expressed in purely kinematic terms using the density relation (2.5). We shall use the above density-independent formulation in deriving separation conditions for moving boundaries in § 2.9.

2.8. *Lagrangian formulation*

In a series of papers, Van Dommelen and coworkers have shown that unsteady separation is best described in the Lagrangian frame, a point of view that we have adopted throughout this paper. Working with Prandtl's boundary-layer equations, Van Dommelen (1981) proposes that fluid-stretching in the wall-normal direction becomes infinitely large at the point of separation. He then uses mass conservation in the Lagrangian variables to explore the implications of his postulate for the derivatives of particle positions with respect to initial states. If $x(t;x_0,y_0,t_0)$ denotes at time t the x coordinate of a fluid particle that started from position (x_0,y_0) at time t_0, Van Dommelen's criterion for boundary-layer separation at point (x,y) at time t reads

$$\frac{\partial x(t;x_0,y_0,t_0)}{\partial x_0} = 0, \qquad \frac{\partial x(t;x_0,y_0,t_0)}{\partial y_0} = 0. \tag{2.39}$$

As we show in Appendix C, these conditions may only be fully satisfied for velocity fields with singularities. Another postulate implicit in (2.39) is that the separation point lies off the wall. By contrast, our separation criteria locate on-wall separation in general two-dimensional Navier–Stokes flows for which the velocity field is known to remain regular.

Below we give a mathematically exact Lagrangian separation criterion for comparison with Van Dommelen's criteria. Our Lagrangian criterion applies to any two-dimensional compressible flow that remains regular along the boundary for all times. As we show in Appendix C, the criterion can be written as

$$\limsup_{t\to-\infty}\left|\frac{\partial x(t;\gamma,0,t_0)}{\partial y_0}\right| < \infty, \tag{2.40}$$

where, as earlier, $(\gamma,0)$ denotes the fixed separation point on the boundary. As in the Eulerian formulation, our Lagrangian separation criterion is approximated by the

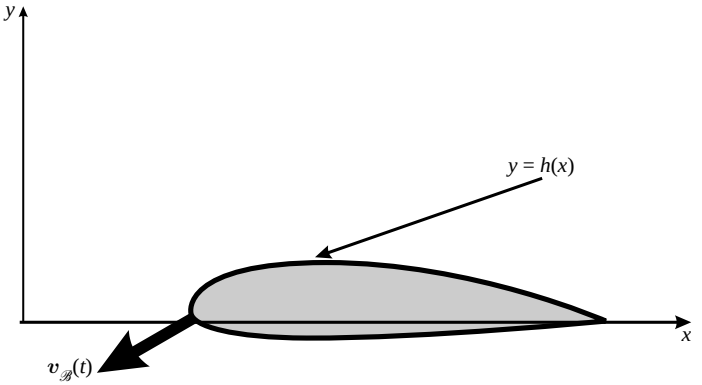

FIGURE 7. Moving boundary defined by the function $y = h(x - \int_{t_0}^{t} u_{\mathscr{B}}(s)\,\mathrm{d}s)$.

effective separation criterion

$$\frac{\partial x(t;\gamma_{eff},0,t_0)}{\partial y_0} = 0, \tag{2.41}$$

which locates an effective separation point $\gamma_{eff}(t_0,t)$ that converges to the true separation point γ as $t \to -\infty$.

Comparing (2.39) and (2.41), we conclude that when applied on the boundary, Van Dommelen's second separation condition in (2.39) coincides asymptotically with the Lagrangian version of our first necessary condition. Once the second condition in (2.39) holds, however, the first condition will never be satisfied for a non-singular velocity field.

2.9. *Separation on moving boundaries of general shape*

Assume now that the velocity field (2.10) satisfies no-slip boundary conditions along a boundary $\mathscr{B}(t)$ that moves with velocity $\boldsymbol{v}_{\mathscr{B}}(t) = (u_{\mathscr{B}}(t), v_{\mathscr{B}}(t))$. We want to find a necessary condition for separation at a point whose relative location is fixed on the moving boundary.

If at time t_0 the boundary – say, a moving airfoil – is represented by a differentiable graph $y = h(x)$, then at a later time t the boundary satisfies

$$y - \int_{t_0}^{t} v_{\mathscr{B}}(s)\,\mathrm{d}s = h\left(x - \int_{t_0}^{t} u_{\mathscr{B}}(s)\,\mathrm{d}s\right), \tag{2.42}$$

as indicated in figure 7.

We now transform the velocity field to the canonical form (2.1) by letting

$$\xi = x - \int_{t_0}^{t} u_{\mathscr{B}}(s)\,\mathrm{d}s, \qquad \eta = y - h(\xi) - \int_{t_0}^{t} v_{\mathscr{B}}(s)\,\mathrm{d}s. \tag{2.43}$$

In terms of the (ξ,η) coordinates, fluid particle motions satisfy

$$\dot{\xi} = \hat{u}(\xi,\eta,t), \quad \dot{\eta} = \hat{v}(\xi,\eta,t), \tag{2.44}$$

where

$$\left.\begin{aligned}\hat{u}(\xi,\eta,t) &= u\left(\xi+\int_{t_0}^{t} u_{\mathscr{B}}(s)\,\mathrm{d}s,\ \eta+h(\xi)+\int_{t_0}^{t} v_{\mathscr{B}}(s)\,\mathrm{d}s,\ t\right)-u_{\mathscr{B}}(t),\\ \hat{v}(\xi,\eta,t) &= v\left(\xi+\int_{t_0}^{t} u_{\mathscr{B}}(s)\,\mathrm{d}s,\ \eta+h(\xi)+\int_{t_0}^{t} v_{\mathscr{B}}(s)\,\mathrm{d}s,\ t\right)-v_{\mathscr{B}}(t)-h'(\xi)\hat{u}(\xi,\eta,t).\end{aligned}\right\} \tag{2.45}$$

The transformed velocity field $(\hat{u}, \hat{v})$ satisfies the boundary conditions

$$\hat{u}(x,0,t)=0, \qquad \hat{v}(x,0,t)=0. \tag{2.46}$$

Furthermore,

$$\hat{u}_\xi+\hat{v}_\eta = u_x+u_y h'+v_y-h'u_y = u_x+v_y, \tag{2.47}$$

thus compressibility or incompressibility is unaffected by the change of coordinates $(x, y) \mapsto (\xi, \eta)$.

Because

$$\left.\begin{aligned}\hat{u}_\eta(\xi,\eta,t) &= u_y\left(\xi+\int_{t_0}^{t} u_{\mathscr{B}}(s)\,\mathrm{d}s,\ \eta+h(\xi)+\int_{t_0}^{t} v_{\mathscr{B}}(s)\,\mathrm{d}s,\ t\right),\\ \hat{v}_\eta(\xi,\eta,t) &= v_y\left(\xi+\int_{t_0}^{t} u_{\mathscr{B}}(s)\,\mathrm{d}s,\ \eta+h(\xi)+\int_{t_0}^{t} v_{\mathscr{B}}(s)\,\mathrm{d}s,\ t\right)-h'(\xi)\hat{u}_\eta(\xi,\eta,t),\end{aligned}\right\} \tag{2.48}$$

the density-independent necessary condition (2.36) – applied in the (ξ, η) co-ordinates – takes the form

$$\limsup_{t\to-\infty}\left|\int_{t_0}^{t} E(\tau,t)\,u_y\left(\gamma+\int_{t_0}^{\tau} u_{\mathscr{B}}(s)\,\mathrm{d}s,\ h(\gamma)+\int_{t_0}^{\tau} v_{\mathscr{B}}(r)\,\mathrm{d}r,\ \tau\right)\mathrm{d}\tau\right|<\infty, \tag{2.49}$$

where

$$\begin{aligned}E(\gamma,\tau,t)=\exp\Bigg(\int_{t_0}^{\tau}\Bigg[&v_y\left(\gamma+\int_{t_0}^{s} u_{\mathscr{B}}(r)\,\mathrm{d}r,\ h(\gamma)+\int_{t_0}^{s} v_{\mathscr{B}}(r)\,\mathrm{d}r,\ s\right)\\ &-h'(\gamma)u_y\left(\gamma+\int_{t_0}^{s} u_{\mathscr{B}}(r)\,\mathrm{d}r,\ h(\gamma)+\int_{t_0}^{s} v_{\mathscr{B}}(r)\,\mathrm{d}r,\ s\right)\Bigg]\,\mathrm{d}s\Bigg).\end{aligned} \tag{2.50}$$

As in the case of flat boundaries, we locate the separation point on general boundaries by computing the effective separation point $\gamma_{eff}(t, t_0)$ for $|t - t_0|$ large enough from the formula

$$\int_{t_0}^{t} E(\gamma_{eff},\tau,t)\,u_y\left(\gamma_{eff}+\int_{t_0}^{\tau} u_{\mathscr{B}}(s)\,\mathrm{d}s,\ h(\gamma_{eff})+\int_{t_0}^{\tau} v_{\mathscr{B}}(r)\,\mathrm{d}r,\ \tau\right)\mathrm{d}\tau=0. \tag{2.51}$$

To evaluate the second necessary condition (2.37) in the present (ξ, η) coordinates, we compute the second derivatives

$$\hat{u}_{\xi\eta}(\xi,\eta,t), \quad \hat{v}_{\xi\eta}(\xi,\eta,t), \quad \hat{v}_{\eta\eta}(\xi,\eta,t), \tag{2.52}$$

in terms of the original velocity field from (2.48). With these expressions, the second separation condition (2.37) becomes a straightforward but lengthy condition, which we omit here for brevity.

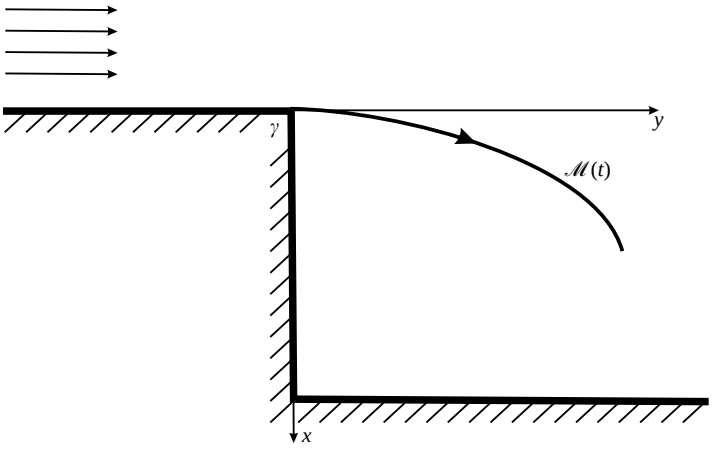

FIGURE 8. Backward facing step, as an example of fixed separation at a corner. Note that the separation is transverse relative to the vertical wall $\{y = 0,\ x \geqslant 0\}$.

2.10. *Separation at a corner*

We now consider flow separation at a corner, i.e. at a point where the boundary fails to be differentiable, but admits two well-defined tangents. Typically, the separation profile will be tangent to one of these tangents, in which case the separation is transverse relative to the other side of the corner. Because our focus so far has been transverse separation, we now consider separation relative to the part of the boundary that lies downstream from the corner.

As earlier, we consider a general boundary of the form $y = h(x, t)$, and assume that the boundary shape h is differentiable in x for all $x > \gamma$, with $x = \gamma$ marking the location of the corner. At the corner γ, we assume that the upper derivative of h,

$$h'(x, t) = \lim_{s \to +0} \frac{h(x + s, t) - h(x, t)}{s}, \tag{2.53}$$

is finite. We seek a separation profile emanating from $(x, y) = (\gamma, h(\gamma, t))$, assuming that $x \geqslant 0$ designates a region downstream of the corner. Thus the separation profile will be transverse to the $x \geqslant 0$ portion of the boundary, as shown in figure 8.

In this setting, our previous arguments for fixed separation carry over without change if we replace differentiation with respect to x with the upper differentiation defined in (2.53). With this slight modification, our formulae for the shape of the separation profile apply to corner separation.

3. Fixed unsteady separation in incompressible flows

In this section, we focus on incompressible flows and show how our theory for fixed unsteady separation simplifies in this case. We also derive a general quartic-order approximation for the separation profile.

3.1. *Set-up*

Consider again the velocity field (2.1), but now with the incompressibility condition

$$u_x + v_y = 0. \tag{3.1}$$

The no-slip boundary conditions again enable us to rewrite the velocity field in the form (2.10), with the equivalent incompressibility condition

$$yA_x + B + yB_y = 0. \tag{3.2}$$

Setting $y = 0$ in this equation gives $B(x, 0, t) \equiv 0$, thus we can further rewrite the velocity field in the form

$$\dot{x} = yA(x, y, t), \qquad \dot{y} = y^2 C(x, y, t), \tag{3.3}$$

where

$$C(x, y, t) = \int_0^1 \int_0^1 v_{yy}(x, spy, t) p \, \mathrm{d}p \, \mathrm{d}s. \tag{3.4}$$

Enforcing the incompressibility condition (3.1) for system (3.3) gives the relation

$$y(A_x + 2C + yC_y) = 0 \tag{3.5}$$

between the functions A and C. Away from the boundary, i.e. for $y > 0$, this relation implies

$$A_x + 2C + yC_y = 0. \tag{3.6}$$

Because A_x, C and C_y are continuous, (3.6) extends to $y = 0$. Therefore, (3.6) must hold all over the fluid, including the boundary.

In our arguments, we will work with the incompressible canonical velocity field (3.3) for simplicity. Alternatively, we could work with the compressible canonical form (2.10) and use the incompressibility condition (3.6), but that approach would quickly lead to intractably complex expressions.

3.2. *Equation for the separation profile*

As in the compressible case, we seek the unsteady separation profile in the form of an unstable manifold satisfying $\xi = x - \gamma = yF(y, t)$. Substituting this relation into (3.3) leads to the equation

$$y[A(yF + \gamma, y, t) - yC(yF + \gamma, y, t)(F + yF_y) - F_t] = 0. \tag{3.7}$$

The bracketed expression must therefore vanish for all $y \geqslant 0$ by continuity, leading to the incompressible separation equation

$$A(yF + \gamma, y, t) - yC(yF + \gamma, y, t)(F + yF_y) - F_t = 0. \tag{3.8}$$

The compressible separation equation (2.14) is equivalent to (3.8) in the case of incompressible flows.

3.3. *Necessary conditions for separation*

Computing the $O(1)$ term in the Taylor expansion of (3.8), we find that

$$\dot{f}_0 = a, \tag{3.9}$$

which implies

$$f_0(t) = f_0(t_0) + \int_{t_0}^{t} a(\tau) \, \mathrm{d}\tau. \tag{3.10}$$

As in the compressible case, we obtain a necessary criterion at the point $(\gamma, 0)$ by requiring $f_0(t)$ to be bounded in backward time:

$$\limsup_{t \to -\infty} \left| \int_{t_0}^{t} u_y(\gamma, 0, \tau) \, \mathrm{d}\tau \right| < \infty. \tag{3.11}$$

In analogy with (2.22), the further necessary condition

$$\int_{t_0}^{-\infty} u_{xy}(\gamma, 0, \tau)\,\mathrm{d}\tau = \infty \tag{3.12}$$

must hold at fixed separation points. Note that, by incompressibility, this last condition is equivalent to

$$\int_{t_0}^{-\infty} v_{yy}(\gamma, 0, \tau)\,\mathrm{d}\tau = -\infty. \tag{3.13}$$

3.4. *Effective separation points*

As noted earlier, the separation criterion (3.11) is unsuitable for direct computations. Instead, we use effective separation points defined as

$$\int_{t_0}^{t} u_y(\gamma_{\mathit{eff}}, 0, s)\,\mathrm{d}s = 0, \tag{3.14}$$

to approximate the location of the actual flow separation. Our argument for the convergence of effective separation points to actual separation points is again valid here.

3.5. *Separation profile up to quartic order*

We now give explicit formulae for the time-dependent coefficients of the quartic separation profile

$$x = \gamma + f_0(t)y + f_1(t)y^2 + \tfrac{1}{2}f_2(t)y^3 + \tfrac{1}{6}f_3(t)y^4. \tag{3.15}$$

While these coefficients are tedious to compute for the compressible case, they become manageable in the present setting. As we show in Appendix B, the coefficients take the following form when evaluated at time t_0:

$$f_0(t_0) = \lim_{t\to-\infty} \frac{\displaystyle\int_{t_0}^{t}\left[a_y(\tau) - 3c(\tau)\int_{t_0}^{\tau} a(s)\,\mathrm{d}s\right]\mathrm{d}\tau}{\displaystyle 3\int_{t_0}^{t} c(\tau)\,\mathrm{d}\tau}, \tag{3.16}$$

$$f_1(t_0) = \lim_{t\to-\infty} \frac{\displaystyle\int_{t_0}^{t}\left\{a_{yy}(\tau) - 8c_y(\tau)f_0(\tau) - 4c_x(\tau)f_0^2(\tau) - 8c(\tau)\int_{t_0}^{\tau}[a_y(s) - 3c(s)f_0(s)]\,\mathrm{d}s\,\mathrm{d}\tau\right\}}{\displaystyle 8\int_{t_0}^{t} c(\tau)\,\mathrm{d}\tau}, \tag{3.17}$$

$$f_2(t_0) = \lim_{t\to-\infty}\left[\frac{\displaystyle\int_{t_0}^{t}\left(\frac{1}{15}a_{yyy} - \frac{1}{3}c_{xx}f_0^3 - c_{xy}f_0^2 - c_{yy}f_0 - 2c_yf_1 - 2c_x\,f_0f_1\right)\mathrm{d}\tau}{\displaystyle\int_{t_0}^{t} c\,\mathrm{d}\tau} + \frac{\displaystyle\int_{t_0}^{t} c\left(\int_{t_0}^{\tau}\left(4c_xf_0^2 + 8c_yf_0 + 8cf_1 - a_{yy}\right)\mathrm{d}s\right)\mathrm{d}\tau}{\displaystyle\int_{t_0}^{t} c\,\mathrm{d}\tau}\right], \tag{3.18}$$

$$f_3(t_0) = \lim_{t\to-\infty}\left[\frac{\displaystyle\int_{t_0}^{t}\left(\frac{1}{24}a_{yyyy} - \frac{1}{4}c_{xxxx}f_0^4 - c_{xxy}f_0^3 - \frac{3}{2}c_{xyy}f_0^2 + c_{yyy}f_0\right)\mathrm{d}\tau}{\displaystyle\int_{t_0}^{t} c\,\mathrm{d}\tau}\right.$$

$$-3\frac{\displaystyle\int_{t_0}^{t}\left(c_{xx}f_0^2 f_1 + 2c_{xy}f_0 f_1 + c_{yy}f_1 + c_x\left[f_1^2 + f_0 f_2\right] + c_y f_2\right)\mathrm{d}\tau}{\displaystyle\int_{t_0}^{t} c\,\mathrm{d}\tau}$$

$$\left.+5\frac{\displaystyle\int_{t_0}^{t} c\left\{\int_{t_0}^{\tau}\left(c_{xx}f_0^3 + 3c_{xy}f_0^2 + 3c_{yy}f_0 + 6c_x f_0 f_1 + 6c_y f_1 + 3cf_2 - \frac{1}{5}a_{yyy}\right)\mathrm{d}s\right\}\mathrm{d}\tau}{\displaystyle\int_{t_0}^{t} c\,\mathrm{d}\tau}\right]. \tag{3.19}$$

4. Unsteady separation from pressure and skin friction

Monitoring and controlling unsteady separation in experiments requires separation criteria phrased in terms of physically measurable quantities. Here we present a formulation of our separation theory in terms of pressure, skin friction, density and viscosity measured along the wall.

We recall that the skin friction $\tau_w(x,t)$ is defined as

$$\tau_w(x,t) = \nu\rho(x,0,t)u_y(x,0,t), \tag{4.1}$$

where ν denotes the kinematic viscosity. Using τ_w, we rewrite the first separation condition (2.21) as

$$\limsup_{t\to-\infty}\left|\int_{t_0}^{t}\frac{\tau_w(\gamma,s)}{\rho^2(\gamma,0,s)}\,\mathrm{d}s\right| < \infty. \tag{4.2}$$

For some $t < t_0$, the effective separation point is then computed from the equation

$$\int_{t_0}^{t}\frac{\tau_w(\gamma_{eff}(t,t_0),s)}{\rho^2(\gamma_{eff}(t,t_0),0,s)}\,\mathrm{d}s = 0, \tag{4.3}$$

thus for incompressible flows, the effective separation point coincides with the point of zero mean-skin-friction. For compressible flows, however, the zero-mean-skin-friction rule is generally inadequate as a true separation indicator: to obtain a good estimate for the separation location, we need to use $1/\rho^2$ as a weight function when integrating the skin friction in time.

For incompressible flows, the second separation criterion (2.22) also admits a simple kinetic formulation. Differentiating equation (4.1) with respect to x, we obtain

$$\tau_w'(x,t) = \tau_w(x,t)\rho_x(x,0)/\rho(x,0) + \nu\rho(x,0)u_{xy}(x,0,t), \tag{4.4}$$

from which we express and substitute u_{xy} into (2.22) to obtain the second kinetic separation criterion

$$\int_{t_0}^{-\infty}\left[\tau_w'(x,\tau)\rho(x,0) - \tau_w(x,\tau)\rho_x(x,0)\right]\mathrm{d}\tau = \infty. \tag{4.5}$$

In addition to these necessary criteria, our separation slope formula also admits a purely kinetic form for incompressible flows. To derive this form, we observe

that along the no-slip boundary $y = 0$, the incompressible Navier–Stokes equations simplify to

$$p_x(x,0,t)/\rho(x,0) = \nu u_{yy}(x,0,t), \qquad v_{yy}(x,0,t) = -u_{xy}(x,0,t), \tag{4.6}$$

with $p(x,y,t)$ denoting the pressure. Combining these formulae with the definitions of $a(\gamma,t)$ and $c(\gamma,t)$, we obtain the kinetic separation slope formula

$$f_0(t_0) = \lim_{t\to-\infty} \frac{\displaystyle\int_{t_0}^{t}\left[\nu p_x(\gamma,0,\tau)\rho^2(\gamma,0) + 3[\tau_w'(\gamma,\tau)\rho(\gamma,0) - \tau_w(\gamma,\tau)\rho_x(\gamma,0)]\int_{t_0}^{\tau}\tau_w(\gamma,\tau)\,\mathrm{d}s\right]\mathrm{d}\tau}{3\nu\rho(\gamma,0)\displaystyle\int_{t_0}^{t}[\tau_w(\gamma,\tau)\rho_x(\gamma,0) - \tau_w'(\gamma,\tau)\rho(\gamma,0)]\,\mathrm{d}\tau}. \tag{4.7}$$

If the initial density of the incompressible fluid is equal to a constant ρ_0 along the wall, then the kinetic separation slope formula takes the simpler form

$$f_0(t_0) = -\lim_{t\to-\infty} \frac{\displaystyle\int_{t_0}^{t}\left[p_x(\gamma,0,\tau) + 3\tau_w'(\gamma,\tau)\int_{t_0}^{\tau}(1/\nu\rho)\tau_w(\gamma,\tau)\,\mathrm{d}s\right]\mathrm{d}\tau}{3\displaystyle\int_{t_0}^{t}\tau_w'(\gamma,\tau)\,\mathrm{d}\tau}. \tag{4.8}$$

Formulae (4.2) and (4.7) show that for incompressible flows, the separation location and slope can both be monitored from pressure and skin friction sensors distributed along the wall.

5. Sufficient conditions for sharp separation

So far we have described necessary features of fixed unsteady separation: if separation takes place at the point $(\gamma,0)$, then conditions (2.21) and (2.22) must hold. As we argue below, a slightly stronger version of this set of conditions turns out to be sufficient: when these stronger conditions are satisfied, they guarantee the existence of a time-dependent nonlinear separation profile anchored to a boundary point.

To motivate these sufficient conditions, we first note that condition (2.21) is general enough to allow for *weak separation*. By weak separation we mean a scenario whereby particles near the separation point may turn back towards the wall for finite periods of time, and are only ejected from a vicinity of the wall asymptotically. Such weak separation behaviour is atypical in observed fluid motion where, once started, separation tends to be *sharp*: particles in a vicinity of the separation point move away monotonically from the wall without turning back.

In this paper, we establish a sufficient criterion for sharp separation. To avoid lengthy technical arguments, we assume that the flow is incompressible. As we prove in Appendix D, sharp incompressible separation takes place if the first necessary condition

$$\limsup_{t\to-\infty}\left|\int_{t_0}^{t}u_y(\gamma,0,s)\,\mathrm{d}s\right| < \infty \tag{5.1}$$

and a stronger version of the second criterion (3.12) both hold. This stronger criterion requires u_{xy} to be negative and uniformly bounded away from zero for all times, i.e.

requires

$$u_{xy}(\gamma, 0, t) < -c_0 < 0. \tag{5.2}$$

For details of the argument, see Appendix D.

As a simple Taylor expansion shows, the quantity $v_{yy}(\gamma, 0, t) = -u_{xy}(\gamma, 0, t)$ is the dominant term in the instantaneous strength of separation. Requiring it to be strictly positive for all times ensures continued ejection of particles (sharp separation) from a vicinity of the wall. By contrast, the incompressible necessary condition (3.12) only requires the asymptotic mean of $v_{yy}(\gamma, 0, t)$ to be strictly positive, and hence allows for weak separation.

6. Separation in flows with simple time dependence

Here, we evaluate our results for three simple classes of flows that produce fixed separation: steady, time-periodic and quasi-periodic flows. In all three cases, separation points and profiles turn out to be exactly computable from finite-time velocity data, and hence the use of effective separation points is unnecessary. In the steady and time-periodic cases, we show how our criteria for the separation location and angle agree with previous results by others. For the quasi-periodic case, no related results are available in the literature.

6.1. *Steady flows*

6.1.1. *Assumptions*

For a steady compressible flow with a horizontal no-slip boundary at $y = 0$, the continuity equation (2.3) yields

$$\rho(x, 0)v_y(x, 0) = 0. \tag{6.1}$$

Because the density of the fluid is non-zero along the boundary, we obtain

$$v_y(x, 0) = 0, \tag{6.2}$$

which also implies

$$v_{xy}(x, 0) = 0. \tag{6.3}$$

Therefore, our main assumptions (2.7)–(2.8) are satisfied for steady flows.

6.1.2. *Separation criteria*

Because the density $\rho(x, y)$ is constant in time, the first separation condition (2.21) becomes

$$\left| \int_{t_0}^{-\infty} u_y(\gamma, 0)\, \mathrm{d}s \right| = \lim_{t \to -\infty} |u_y(\gamma, 0)(t_0 - t)| < \infty. \tag{6.4}$$

This condition is equivalent to

$$u_y(\gamma, 0) = 0, \tag{6.5}$$

which is Prandtl's classic necessary condition for steady separation at $(\gamma, 0)$ (cf. (1.1)).

Differentiating the continuity equation (2.3) with respect to y, we obtain

$$\rho(\gamma, 0)[u_{xy}(\gamma, 0) + v_{yy}(\gamma, 0)] = 0, \tag{6.6}$$

which implies

$$u_{xy}(\gamma, 0) = -v_{yy}(\gamma, 0). \tag{6.7}$$

Thus, our second separation criterion (2.22) can be written as

$$\int_{t_0}^{-\infty} [u_{xy}(\gamma,0) - v_{yy}(\gamma,0)]\,\mathrm{d}\tau = \lim_{t\to-\infty} 2\int_{t_0}^{-\infty} u_{xy}(\gamma,0)\,\mathrm{d}\tau$$
$$= \lim_{t\to-\infty} 2u_{xy}(\gamma,0)(t-t_0) = \infty, \tag{6.8}$$

implying

$$u_{xy}(\gamma,0) < 0. \tag{6.9}$$

This is Prandtl's second condition for steady separation (cf. (1.1)).

6.1.3. *Separation profile*

The slope of the separation profile is given by formula (2.30), which now simplifies to

$$f_0(t_0) = \lim_{t\to-\infty} \frac{-\int_{t_0}^{t} a_y(\tau)\,\mathrm{d}\tau}{\int_{t_0}^{t} [a_x(\tau) - b_y(\tau)]\,\mathrm{d}\tau} = -\frac{u_{yy}(\gamma,0)}{3u_{xy}(\gamma,0)}, \tag{6.10}$$

where we have used (6.5) and (6.7). This last equation agrees with a classic result, Lighthill's formula for the separation slope in steady flows (Lighthill 1963). Higher-order approximations for steady separation profiles can be derived following §§2 and 3.

6.2. *Time-periodic flows*

6.2.1. *Assumptions*

If the velocity field $\boldsymbol{v} = (u, v)$ is T-periodic in time, then $\boldsymbol{v}$ and its derivatives admit Fourier expansions in time. In particular, $v_y(x, y, t)$ can be written as the sum of a time-independent mean and a time-dependent oscillating part:

$$v_y(x,y,t) = \bar{v}_y(x,y) + \tilde{v}_y(x,y,t), \tag{6.11}$$

where

$$\bar{v}_y(x,y) = \frac{1}{T}\int_0^T v_y(x,y,t)\,\mathrm{d}t, \qquad \int_0^T \tilde{v}_y(x,y,t)\,\mathrm{d}t = 0. \tag{6.12}$$

The first major assumption in our fixed separation study was (2.7), which now takes the particular form

$$\limsup_{t\to-\infty}\left|\int_{t_0}^{t} v_y(x,0,s)\,\mathrm{d}s\right| = \limsup_{t\to-\infty}\left|\bar{v}_y(x,0)\,(t-t_0) + \int_{t_0}^{t}\tilde{v}_y(x,0,s)\,\mathrm{d}s\right| < \infty. \tag{6.13}$$

Because $\tilde{v}_y(x, y, t)$ is a zero-mean periodic function of t, the integral $\int_{t_0}^{t}\tilde{v}_y(x,y,s)\,\mathrm{d}s$ is also a zero-mean periodic function of t, and hence remains bounded for all t. Then, in view of the density formula (2.5), assumption (2.7) is equivalent to

$$\int_0^T v_y(\gamma,0,t)\,\mathrm{d}t = 0. \tag{6.14}$$

We stress that without this last assumption, the density at the separation point would tend to zero or infinity. Repeating the above argument for assumption (2.8), we obtain

$$\int_0^T v_{xy}(\gamma,0,t)\,\mathrm{d}t = 0, \tag{6.15}$$

which prevents the unbounded growth of the wall-tangential density gradient at the point of separation.

6.2.2. *Separation criteria*

Under assumption (6.14), the first separation condition (2.21) becomes

$$\limsup_{t\to-\infty}\left|\int_{t_0}^{t}\frac{u_y(\gamma,0,s)}{\rho(\gamma,0,s)}\,\mathrm{d}s\right|<\infty. \tag{6.16}$$

Again, the integrand in this condition is a T-periodic function, thus the integral only remains bounded if

$$\int_0^T\frac{u_y(\gamma,0,t)}{\rho(\gamma,0,t)}\,\mathrm{d}t=0, \tag{6.17}$$

giving a general criterion for separation in two-dimensional time-periodic flows.

For incompressible time-periodic flows, the relevant first separation criterion is (3.11), which can only hold if

$$\int_0^T u_y(\gamma,0,t)\,\mathrm{d}t=0. \tag{6.18}$$

This agrees with the result of Shariff *et al.* (1991) on the location of unstable manifolds in two-dimensional incompressible flows with a no-slip boundary. While Yuster & Hackborn (1997) gave compressible counter-examples to the main assertion in the argument of Shariff *et al.*, our results justify the assertion for time-periodic incompressible flows.

Our second separation criterion can also be evaluated by splitting the integrand in (2.22) into a mean and an oscillating part. This time, however, the mean must be negative for the criterion to be satisfied, thus

$$\int_0^T\left[\frac{1}{\rho(t)}(u_{xy}(\gamma,0,t)-v_{yy}(\gamma,0,t))-2v_{xy}(\gamma,0,t)\int_{t_0}^{t}\frac{u_y(\gamma,0,s)}{\rho(\gamma,0,s)}\,\mathrm{d}s\right]\mathrm{d}t<0 \tag{6.19}$$

must hold for all t_0. For incompressible flows, this criterion simplifies to

$$\int_0^T u_{xy}(\gamma,0,t)\,\mathrm{d}t<0, \tag{6.20}$$

as we readily deduce from (3.12).

Time-periodic flows illustrate that the lim sup operation cannot be replaced by lim in the separation criterion (2.21). Indeed, at a fixed separation point γ, the left-hand side of formula (3.11) becomes

$$\limsup_{t\to-\infty}\left|\int_{t_0}^{t}u_y(\gamma,0,\tau)\,\mathrm{d}\tau\right|=\limsup_{t\to-\infty}\left|\int_{t_0}^{t}\tilde{u}_y(x,y,\tau)\,\mathrm{d}\tau\right|, \tag{6.21}$$

and the integrand in this formula will have no limit as $t\to-\infty$ for an unsteady time-periodic velocity field.

6.2.3. *Separation profile*

Based on the above arguments, all our asymptotic formulae for the derivatives of the separation profile simplify to integrals over one period. For instance, the separation angle formula (2.30) becomes

$$f_0(t_0)=\frac{\rho(t_0)\displaystyle\int_0^T\left[\frac{b_y(t)-a_x(t)}{\rho(t)}\int_{t_0}^{t}\frac{a(s)}{\rho(s)}\,\mathrm{d}s+b_x(t)\left(\int_{t_0}^{t}\frac{a(s)}{\rho(s)}\,\mathrm{d}s\right)^2-\frac{a_y(t)}{\rho^2(t)}\right]\mathrm{d}t}{\displaystyle\int_0^T\left[\frac{a_x(t)-b_y(t)}{\rho(t)}-2b_x(t)\int_{t_0}^{t}\frac{a(s)}{\rho(s)}\,\mathrm{d}s\right]\mathrm{d}t}. \tag{6.22}$$

For incompressible flows, this formula further simplifies to

$$f_0(t_0) = \frac{\displaystyle\int_0^T \left[a_y(t) - 3c(t) \int_{t_0}^t a(s)\,\mathrm{d}s \right] \mathrm{d}t}{\displaystyle 3\int_0^T c(t)\,\mathrm{d}t}, \tag{6.23}$$

as we see from (3.16). In terms of the original velocity field, condition (6.23) reads

$$f_0(t_0) = \frac{\displaystyle\int_0^T u_{yy}(\gamma,0,t)\,\mathrm{d}t \; - 3\int_{t_0}^t v_{yy}(\gamma,0,t) \int_0^T u_y(\gamma,0,s)\,\mathrm{d}s\,\mathrm{d}t}{\displaystyle 3\int_0^T v_{yy}(\gamma,0,t)\,\mathrm{d}t}. \tag{6.24}$$

Using the incompressibility condition $v_{yy} = -u_{xy}$, reparameterizing the domain of the double integral, and setting $t_0 = 0$, we can further rewrite (6.4) as

$$f_0(0) = \frac{\displaystyle 3\int_0^T u_y(\gamma,0,t) \int_0^t u_{xy}(\gamma,0,s)\,\mathrm{d}s\,\mathrm{d}t - \int_0^T u_{yy}(\gamma,0,t)\,\mathrm{d}t}{\displaystyle 3\int_0^T u_{xy}(\gamma,0,t)\,\mathrm{d}t}, \tag{6.25}$$

which agrees with formula (19) of Shariff *et al.* (1991). As we have mentioned above, while Yuster & Hackborn (1997) give compressible counter-examples to the general assertion that Shariff *et al.* use to derive the above formula, our results show that their assertion is correct for incompressible time-periodic flows.

The incompressible formulae (3.17)–(3.19) simplify in the same fashion as (3.16) simplifies to (6.23): the limit of the quotient of long-term averages is replaced by the quotient of averages over one period.

6.3. *Quasi-periodic flows*

Quasi-periodic flows still display simple time-dependence, yet cannot be studied through the repeated iteration of a single period-T map. For this reason, even partial or *ad hoc* separation results have been unavailable for quasi-periodic separation. Here, we show how our general separation criteria translate to simple formulae in the quasi-periodic case.

Many canonical separation problems, such as separation behind a cylinder or a backward facing step, admit a finite number of dominant frequencies in their Fourier spectrum. Such flows are approximated well by quasi-periodic velocity fields, which are amenable to the criteria described below.

6.3.1. *Assumptions*

Let $\omega_1, \omega_2, \ldots, \omega_m$ be m numbers that are rationally independent, i.e. admit no vanishing linear combination with rational coefficients. We say that the original velocity field $(u(x, y, t), v(x, y, t))$ is quasi-periodic in time with frequencies $\omega_1, \ldots, \omega_m$, if we can write

$$\left.\begin{aligned} u(x, y, t) &= U(x, y, \omega_1 t, \ldots, \omega_m t), \\ v(x, y, t) &= V(x, y, \omega_1 t, \ldots, \omega_m t), \end{aligned}\right\} \tag{6.26}$$

where the functions $U(x, y, \phi_1, \ldots, \phi_m)$, and $V(x, y, \phi_1, \ldots, \phi_m)$ are 2π-periodic in each of the arguments $\phi_1, \ldots, \phi_m$.

Quasi-periodic velocity fields can be Fourier expanded in terms of the angular arguments ϕ_i, thus we can write

$$\left.\begin{aligned} u(x, y, t) &= \overline{u(x, y, t)} + \tilde{u}(x, y, t), \\ v(x, y, t) &= \overline{v(x, y, t)} + \tilde{u}(x, y, t), \end{aligned}\right\} \tag{6.27}$$

where

$$\left.\begin{aligned} \overline{u(x, y, t)} &= \frac{1}{(2\pi)^m} \int_0^{2\pi} \cdots \int_0^{2\pi} U(x, y, \phi_1, \ldots, \phi_m)\, \mathrm{d}\phi_1 \ldots \mathrm{d}\phi_m, \\ \overline{v(x, y, t)} &= \frac{1}{(2\pi)^m} \int_0^{2\pi} \cdots \int_0^{2\pi} V(x, y, \phi_1, \ldots, \phi_m)\, \mathrm{d}\phi_1 \ldots \mathrm{d}\phi_m, \end{aligned}\right\} \tag{6.28}$$

and $(\tilde{u}(x, y, t), \tilde{u}(x, y, t))$ denotes the bounded oscillatory part of the velocity. Just as in the periodic case, we perform a decomposition into mean and oscillating parts for the quantities featured in (2.7)–(2.8), and obtain

$$\overline{v_y(\gamma, 0, t)} = 0, \qquad \overline{v_{xy}(\gamma, 0, t)} = 0, \tag{6.29}$$

as the main physical assumptions for our theory. Again, these assumptions ensure the boundedness of the density and the density gradient along the wall.

6.3.2. *Separation criteria*

Following the arguments we gave in the periodic case, we deduce the two separation criteria

$$\left.\begin{aligned} \overline{\frac{u_y(\gamma, 0, t)}{\rho(\gamma, 0, t)}} &= 0, \qquad (6.30) \\ \overline{\frac{u_{xy}(\gamma, 0, t) - v_{yy}(\gamma, 0, t)}{\rho(\gamma, 0, t)} - 2v_{xy}(\gamma, 0, t) \int_{t_0}^{t} \frac{u_y(\gamma, 0, s)}{\rho(\gamma, 0, s)}\, \mathrm{d}s} &< 0. \qquad (6.31) \end{aligned}\right\}$$

Here, the second criterion must be satisfied for all $t_0 > 0$.

6.3.3. *Separation profile*

Quasi-periodic separation profiles obey formulae similar to their periodic counterparts. We simply take the periodic formulae and replace single-phase averaging over $[0, T]$ with multi-phase averaging as defined above. For instance, the separation slope now obeys the formula

$$f_0(t_0) = \rho(t_0) \frac{\overline{\dfrac{b_y(t) - a_x(t)}{\rho(t)} \displaystyle\int_{t_0}^{t} \frac{a(s)}{\rho(s)}\, \mathrm{d}s + b_x(t) \left(\int_{t_0}^{t} \frac{a(s)}{\rho(s)}\, \mathrm{d}s \right)^2 - \frac{a_y(t)}{\rho^2(t)}}}{\overline{\dfrac{a_x(t) - b_y(t)}{\rho(t)} - 2b_x(t) \displaystyle\int_{t_0}^{t} \frac{a(s)}{\rho(s)}\, \mathrm{d}s}}, \tag{6.32}$$

simplifying to

$$f_0(t_0) = \frac{\overline{a_y(t) - 3c(t) \displaystyle\int_{t_0}^{t} a(s)\, \mathrm{d}s}}{3\overline{c(t)}} \tag{6.33}$$

in the incompressible case. We omit the remaining higher-order expressions for brevity.

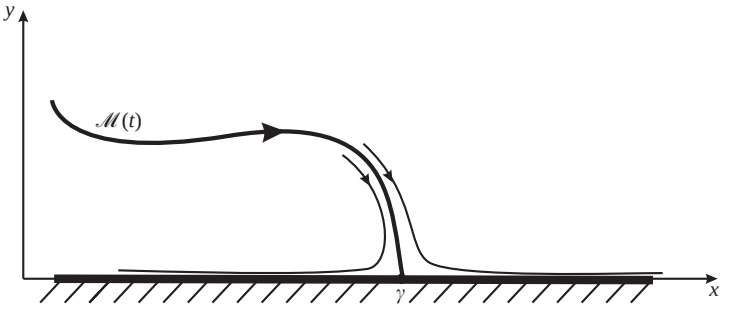

FIGURE 9. Reattachment profile as time-dependent stable manifold for the boundary point γ.

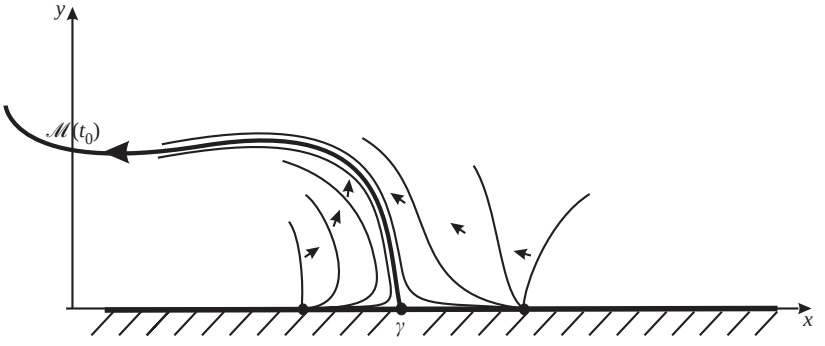

FIGURE 10. Behaviour of wall-bound material lines near a reattachment profile in backward time.

7. Unsteady flow reattachment

We view reattachment profiles as material lines that shrink to a single boundary point, the point of reattachment, as $t \to \infty$. Thus, in dynamical systems terms, a reattachment profile is a time-dependent *stable manifold*, or *repelling material line*, as shown in figure 9.

Material lines that emanate from generic boundary points become asymptotically tangent to the boundary in the $t \to -\infty$ limit, as shown in figure 10. By contrast, all derivatives of fixed reattachment profiles at $y = 0$ stay bounded for all past times. As in the case of fixed separation, we enforce this boundedness property on the solutions of the separation equation (2.14) to deduce

$$\limsup_{t \to -\infty} \left| \int_{t_0}^{t} \frac{u_y(\gamma, 0, s)}{\rho(\gamma, 0, s)} \, \mathrm{d}s \right| < \infty, \tag{7.1}$$

the first necessary condition for fixed unsteady reattachment at $(\gamma, 0)$.

Effective reattachment points can be defined through the formula

$$\int_{t_0}^{t} \frac{u_y(\gamma_{eff}(t, t_0), 0, s)}{\rho(\gamma(t, t_0), 0, s)} \, \mathrm{d}s = 0, \tag{7.2}$$

and they will again converge to actual fixed reattachment points as $t \to -\infty$.

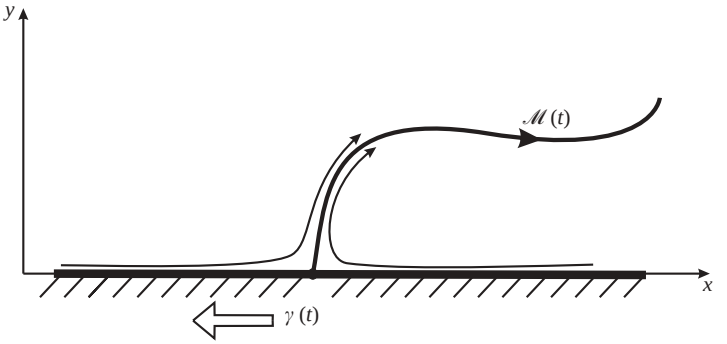

FIGURE 11. Moving separation along a no-slip boundary.

As for a second necessary criterion for unsteady reattachment, we follow the argument in Appendix A to find that

$$\int_{t_0}^{-\infty} \left[\frac{u_{xy}(\gamma,0,\tau) - v_{yy}(\gamma,0,\tau)}{\rho(\gamma,0,\tau)} - 2v_{xy}(\gamma,0,\tau) \int_{t_0}^{\tau} \frac{u_y(\gamma,0,s)}{\rho(\gamma,0,s)}\,\mathrm{d}s \right] \mathrm{d}\tau = -\infty. \quad (7.3)$$

Note that this criterion requires convergence to $-\infty$, as opposed to $+\infty$ in the case of separation. The reason for this difference is that nearby material lines are not repelled but attracted by reattachment profiles in backward time, as shown in figure 10.

Finding the shape of fixed reattachment profiles is more difficult. The reason is that all material lines anchored at the reattachment point are attracted to the reattachment profile in backward time, and hence all admit bounded derivatives at $y=0$ as $t \to -\infty$. For this reason, our successive calculation of derivatives (see Appendix B) fails for reattachment. Exceptions are time-periodic and quasi-periodic flows, for which formulae (6.22), (6.23) and (6.32) remain equally valid in the case of reattachment.

A way to address the above difficulty is to treat fixed reattachment as a special case of moving reattachment. Then the moving separation algorithm described in § 8.1 renders a convergent approximation for the fixed separation profile for increasing values of the present time t_0.

8. Moving separation and reattachment

Moving separation points are commonly observed under varying flow conditions, such as increasing Reynolds numbers in a flow past a cylinder. By moving separation, we mean separation of varying location, which includes the case of disappearing and reappearing separation points. Here, we only discuss moving separation along a flat boundary (figure 11), because the results extend to general boundaries via the approach of § 2.9. For simplicity, we shall assume that the flow is incompressible.

First, we stress that classical invariant manifolds are inadequate for describing moving separation: if particles are to separate from the wall along an attracting material line (a classical unstable manifold), then the point of attachment of the material line on the boundary cannot move owing to the no-slip boundary condition. A similar argument shows that moving reattachment cannot be understood via classical stable manifolds.

The key to understanding moving separation is a recent development in dynamical systems, the concept of *finite-time invariant manifolds* (Haller & Poje 1998; Haller 2000, 2001). A finite-time unstable manifold is a material curve that acts as an unstable manifold for a fixed point only over a finite time interval $\mathscr{I}$. In more physical terms, a finite-time unstable manifold is a material line that attracts all nearby fluid particles over $\mathscr{I}$.

When a finite-time unstable manifold ceases to attract, another nearby material line may become attracting. Then the second material line will act as a separation profile for a while, attracting all nearby material lines, including the one that used to be the separation profile. Later, the second material line may also lose its attracting property, and give its place to a nearby third material line that has just become attracting.

If the above process repeats itself, we observe a sliding separation point created by attachment points of different material lines, each of which acts as a finite-time separation profile. Similarly, moving reattachment can be thought of as the sliding of finite-time attracting material lines along a no-slip wall.

8.1. *Heuristic necessary condition*

Here we give a numerically assisted necessary condition for moving separation in incompressible flows. This criterion assumes that the backward-time integral of the skin friction has a well-defined mean component that can be extracted numerically or analytically. The criterion is heuristic in that it does not address the existence of a finite-time invariant manifold; it simply assumes the presence of a moving point at which the fluid breaks away from the boundary.

Consider a moving separation point that lies at $x = \gamma(t_0)$ at time t_0. For concreteness, assume that the instantaneous velocity of the separation profile is negative, as shown in figure 12. Let $l_1(t)$ be a material line based at a boundary point x_1 that is on the left-hand side of the moving separation profile at time t_0. The motion of $l_1(t)$ is typically aperiodic, but for the separation to be observable in the Lagrangian frame, the mean component of the slope of $l_1(t)$ must grow; we assume that this is the case.

In our arguments below, the *mean component* of a function $f(t)$ (denoted $\langle f\rangle(t)$) will be a low-order polynomial least-squares fit to sampled values of $f(t)$. The sampled values are taken from the interval $[0, T]$, where T and the number of samples are as large as possible. In analytic examples, the mean component may be exactly identifiable without a numerical least-squares fit (for example, $\langle t + \sin t\rangle = t$).

Because the separation profile repels $l_1(t)$ in backward time, the mean component of the slope of $l_1(t)$ relative to the vertical will decrease for decreasing $t < t_0$ values, as shown schematically in figure 12. By contrast, the mean slope of a material line $l_2(t)$ anchored at the point x_2 on the right-hand side of the profile will initially grow in backward time. This trend changes once the backward-moving profile passes x_2: the mean component of the slope of $l_2(t)$ will then decrease for further decreasing values of t (see figure 12).

As a consequence, the derivative

$$\frac{\mathrm{d}}{\mathrm{d}T}[\langle\Delta\alpha\rangle(x, t_0 - T)]_{T=0} \tag{8.1}$$

of the mean-angle-change function $\langle\Delta\alpha\rangle(x, t_0 - T)$ changes sign from negative to positive at the moving separation point $x = \gamma(t_0)$. Thus, in the case of non-degenerate moving separation, $(\mathrm{d}/\mathrm{d}T)[\langle\Delta\alpha\rangle(x, t_0 - T)]_{T=0}$ has a *transverse zero* at $x = \gamma(t_0)$. (With the customary mean definition $\langle\Delta\alpha\rangle = (1/t)\int_0^t \Delta\alpha(\tau)\,\mathrm{d}\tau$, this last conclusion would

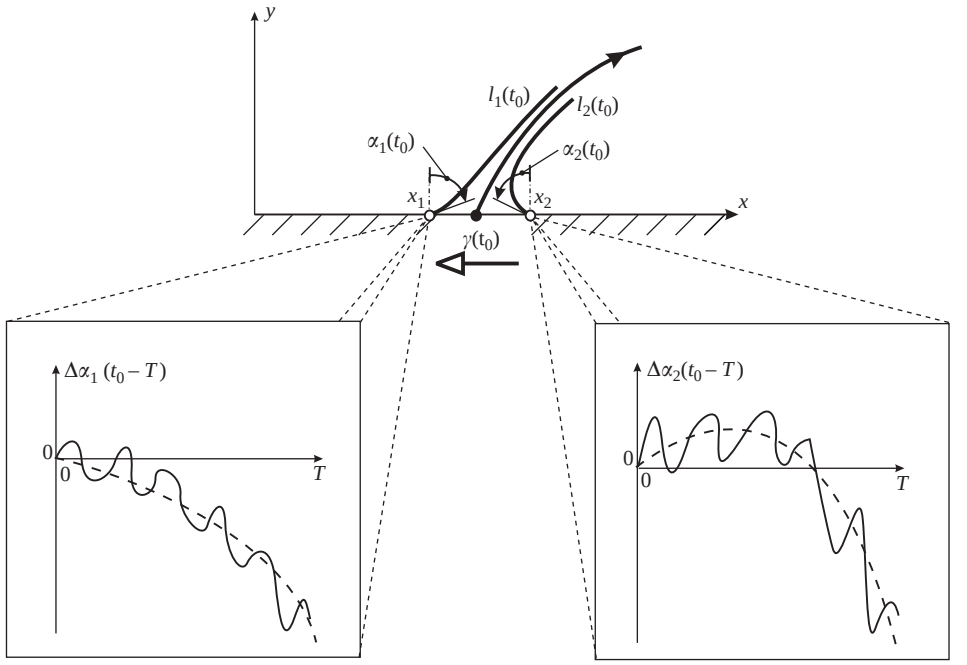

FIGURE 12. Backward-time change in the slope of two material lines lying instantaneously on different sides of a moving separation point. Here $\alpha_i(t)$ denotes the angle enclosed by the material line $l_i(t)$ with the wall at the point x_i. Dashed line indicates the mean evolution of the angle change function $\Delta\alpha_i(t) = \alpha_i(t) - \alpha_i(t_0)$.

be invalid: figure 12 shows a case where $(1/t)\int_0^t \Delta\alpha(\tau)\,\mathrm{d}\tau$ grows initially on both sides of the separation profile.)

The slope of any wall-bound material line satisfies the expression (2.20). In this expression, the first term is constant for incompressible flow, and hence any change in the mean slope comes entirely from the second integral term. Thus a non-degenerate sign change in (8.1) means a transverse zero at $x = \gamma(t_0)$ for the function

$$M_{t_0}(x) = \frac{\mathrm{d}}{\mathrm{d}T}\left\langle \int_{t_0}^{t_0-T} u_y(x, 0, s)\,\mathrm{d}s \right\rangle_{T=0}. \tag{8.2}$$

Such a transverse zero exists at $\gamma(t_0)$ if

$$\frac{\mathrm{d}}{\mathrm{d}T}\left\langle \int_{t_0}^{t_0-T} u_y(\gamma(t_0), 0, s)\,\mathrm{d}s \right\rangle_{T=0} = 0, \quad \frac{\mathrm{d}}{\mathrm{d}T}\left\langle \int_{t_0}^{t_0-T} u_{xy}(\gamma(t_0), 0, s)\,\mathrm{d}s \right\rangle_{T=0} > 0. \tag{8.3}$$

These two conditions give an extension of Prandtl's necessary criteria to moving separation. For moving reattachment, the criteria become

$$\frac{\mathrm{d}}{\mathrm{d}T}\left\langle \int_{t_0}^{t_0-T} u_y(\gamma(t_0), 0, s)\,\mathrm{d}s \right\rangle_{T=0} = 0, \quad \frac{\mathrm{d}}{\mathrm{d}T}\left\langle \int_{t_0}^{t_0-T} u_{xy}(\gamma(t_0), 0, s)\,\mathrm{d}s \right\rangle_{T=0} < 0. \tag{8.4}$$

Recall that $\langle g\rangle(x, t_0, \cdot)$ is a low-order polynomial least-squares fit to sampled values of $g(x, t_0, \cdot)$ over a T interval as large as possible. In practice, this means a least-squares polynomial fit for g values up to $T = t_0 - t_{00}$, where t_{00} is the earliest time at

which velocity data is available. For a faithful approximation of $\langle g \rangle$, the order of the least-squares polynomial should be low relative to the number of sampled values for g. In our later numerical experiments, the order three or four was selected.

With increasing T, $\langle g \rangle$ gives an increasingly accurate representation of the mean evolution of $\int u_y \, \mathrm{d}s$. As a result, transverse zeros of $M_{t_0}(x)$ converge to moving separation or reattachment points as the present time t_0 becomes sufficiently far from t_{00}.

The derivatives of a moving separation profile at the wall can be determined by repeating the argument leading to (8.2). For instance, the mean curvature of $l_1(t)$ decreases in backward time for $t < t_0$, while the mean curvature of $l_2(t)$ only decreases in backward time after an initial period of increase. Assuming incompressibility, we use the curvature formula (12.6) to find that

$$N_{t_0}(x) = \frac{\mathrm{d}}{\mathrm{d}T} \left\langle \int_{t_0}^{t_0-T} \left[u_{yy}(x,0,\tau) - 3v_{yy}(x,0,\tau) \left(f_0(t_0) + \int_{t_0}^{\tau} u_y(x,0,s)\,\mathrm{d}s \right) \right] \mathrm{d}\tau \right\rangle_{T=0} \tag{8.5}$$

has a transverse zero at $x = \gamma(t_0)$, with $f_0(t_0)$ denoting the slope of the separation profile at $t = t_0$. As a result, we obtain

$$f_0(t_0) = \frac{(\mathrm{d}/\mathrm{d}T) \left\langle \int_{t_0}^{t_0-T} \left[u_{yy}(\gamma(t_0),0,\tau) - 3v_{yy}(\gamma(t_0),0,\tau) \int_{t_0}^{\tau} u_y(\gamma(t_0),0,s)\,\mathrm{d}s \right] \mathrm{d}\tau \right\rangle_{T=0}}{3(\mathrm{d}/\mathrm{d}T) \left\langle \int_{t_0}^{t_0-T} v_{yy}(\gamma(t_0),0,\tau)\,\mathrm{d}\tau \right\rangle_{T=0}}. \tag{8.6}$$

Higher derivatives of the moving separation profile are obtained in a similar fashion.

As opposed to the case of fixed separation profiles, (8.6) is equally valid for moving flow reattachment. This is because (8.6) follows from a bifurcation in short-term material line behaviour that is also present in moving reattachment.

We recall that moving separation profiles are inherently non-unique. The formulae given above single out the separation profile that attracts nearby material lines at the highest rate. The numerical extraction of the mean component $\langle g \rangle$ is also a non-unique procedure, but it is the bifurcation of $\langle g \rangle$ that defines the moving separation location, not the actual values of $\langle g \rangle$. In our numerical experiments (see § 9) we found the separation location to be robust with respect to changes in the order of the polynomial least-squares fit producing $\langle g \rangle$.

8.2. *Analytic sufficient condition*

Moving separation can also be treated in rigorous analytic terms without assuming a well-defined mean for the skin friction integral. First, for the present time t_0, we compute the effective separation point $\gamma_{eff}(t, t_0)$ for all available $t < t_0$, then identify the upper and lower bounds

$$\gamma_+(t, t_0) = \sup_{s \in [t, t_0)} \gamma_{eff}(s, t_0), \qquad \gamma_-(t, t_0) = \inf_{s \in [t, t_0)} \gamma_{eff}(s, t_0), \tag{8.7}$$

on $\gamma_{eff}(t, t_0)$. Let the maximal x distance travelled by $\gamma_{eff}(s, t_0)$ over the interval $[t, t_0)$ be denoted by

$$\delta(t, t_0) = \gamma_+(t, t_0) - \gamma_-(t, t_0), \tag{8.8}$$

which is the length of the interval

$$I(t, t_0) = [\gamma_-(t, t_0), \gamma_+(t, t_0)]. \tag{8.9}$$

Finally, assume that the flow is incompressible.

In Appendix E, we prove the existence of finite-time sharp separation at the point

$$\gamma(t_0) = \tfrac{1}{2}[\gamma_+(t_0 - T_m(t_0), t_0) + \gamma_-(t_0 - T_m(t_0), t_0)], \tag{8.10}$$

where $T_m(t_0)$ is the smallest time for which

$$\tfrac{1}{2}\delta(t_0 - T_m(t_0), t_0) \int_{t_0 - T_m(t_0)}^{t_0} \max_{x \in I(t_0 - T_m(t_0), t_0)} |u_{xy}(x, 0, t)| \, \mathrm{d}t = 1, \tag{8.11}$$

$$\max_{x \in I(t_0 - T_m(t_0), t_0)} u_{xy}(x, 0, t) < 0, \quad t \in [t_0 - T_m(t_0), t_0]. \tag{8.12}$$

The above conditions distinguish one finite-time unstable manifold out of the infinitely many near the moving separation point. For specific velocity fields, the conditions may be further sharpened (see Appendix E). A similar result holds for moving reattachment points, except that the second condition in (8.11) is replaced by

$$\max_{x \in I(t_0 - T_m(t_0), t_0)} u_{xy}(x, 0, t) > 0, \quad t \in [t_0 - T_m(t_0), t_0]. \tag{8.13}$$

To obtain derivatives of the moving separation profile at time t_0, we use the time scale $T_m(t_0)$ to evaluate our earlier derivative formulae for fixed separation. For instance, if the flow is incompressible, we use the finite-time version of (3.16) to deduce the moving separation slope formula

$$f_0(t_0) = \frac{\displaystyle\int_{t_0}^{t_0 - T_m(t_0)} \left[a_y(\tau) - 3c(\tau) \int_{t_0}^{\tau} a(s) \, \mathrm{d}s \right] \mathrm{d}\tau}{\displaystyle 3 \int_{t_0}^{t - T_m(t_0)} c(\tau) \, \mathrm{d}\tau}. \tag{8.14}$$

Again, recall that moving separation profiles are non-unique. For any present time t_0, the above criterion singles out the profile that has remained close to an effective separation point $\gamma_{eff}(t, t_0)$ for the longest time.

9. An example: unsteady separation bubble at a no-slip wall

In this section, we test our unsteady separation and reattachment formulae on variants of an unsteady separation bubble flow derived by Ghosh *et al.* (1998). Ghosh *et al.* use the algorithm of Perry & Chong (1986) to derive a low-order approximation to separation bubble solutions of the Navier–Stokes equations. Simple but dynamically relevant, this flow model allows a detailed comparison between our theory and actual flow separation displayed by fluid particles. Numerically more challenging flows will be treated elsewhere.

9.1. *Time-periodic separation bubble*

We first consider the original velocity field derived by Ghosh *et al.* (1998) for the study of passive scalar transport near an unsteady separation bubble. The velocity field is of the form

$$\left.\begin{aligned} u(x, y, t) &= -y + 3y^2 + x^2 y - \tfrac{2}{3}y^3 + \beta x y \sin \omega t, \\ v(x, y, t) &= -xy^2 - \tfrac{1}{2}\beta y^2 \sin \omega t, \end{aligned}\right\} \tag{9.1}$$

with the wall located at $y=0$. Because the flow is incompressible, our main assumptions (6.14) and (6.15) for time-periodic flows are satisfied.

Evaluating conditions (6.18) and (6.20), we obtain

$$\left.\begin{aligned}\int_0^T u_y(\gamma,0,t)\,\mathrm{d}t &= \int_0^T(-1+\gamma^2+\beta\gamma\sin\omega t)\,\mathrm{d}t = (\gamma^2-1)\frac{2\pi}{\omega},\\ \int_0^T v_{yy}(\gamma,0,t)\,\mathrm{d}t &= \int_0^T(-2\gamma-\beta\sin\omega t)\,\mathrm{d}t = -2\gamma\frac{2\pi}{\omega},\end{aligned}\right\} \tag{9.2}$$

and hence fixed separation points must satisfy $|\gamma| = 1$ and $\gamma < 0$, and fixed reattachment points must satisfy $|\gamma| = 1$ and $\gamma > 0$. Separation and reattachment points must therefore lie at

$$\gamma = -1, \qquad \gamma = +1, \tag{9.3}$$

respectively, in agreement with the numerical observation of Ghosh *et al.*

At time t, the derivatives of the separation profile emanating from $(x, y) = (-1, 0)$ obey (3.16)–(3.19). Because the velocity field is time-periodic, (3.16)–(3.19) simplify to quotients of averages over one period, as we remarked at the end of § 6.2. Computing these averages, we find that

$$\left.\begin{aligned}
f_0(t) &= 1+\frac{\beta}{\omega}\cos\omega t,\\
f_1(t) &= \frac{1}{3}-\frac{\beta^2}{2\omega^2}-\frac{3\beta}{2\omega}\cos\omega t-\frac{4\beta}{\omega^2}\sin\omega t-\frac{3\beta^2}{8\omega^2}\cos 2\omega t,\\
f_2(t) &= \frac{2}{3}+\frac{5\beta^2}{2\omega^2}+\frac{\beta}{\omega}\left(\frac{5}{4}\frac{\beta^2}{\omega^2}-\frac{24}{\omega^2}-\frac{4}{3}\right)\cos\omega t+\frac{20\beta}{\omega^2}\sin\omega t\\
&\quad+\frac{3\beta^2}{2\omega^2}\cos 2\omega t+\frac{11\beta^2}{2\omega^3}\sin 2\omega t+\frac{\beta^3}{4\omega^3}\cos 3\omega t,\\
f_3(t) &= \frac{7}{3}+\frac{33}{8}\frac{\beta^2}{\omega^2}-\frac{237}{128}\frac{\beta^4}{\omega^4}+\frac{135}{2}\frac{\beta^2}{\omega^4}+\frac{\beta}{\omega^2}\left(\frac{360}{\omega^2}-\frac{75}{4}\frac{\beta^2}{\omega^2}-15\right)\sin\omega t\\
&\quad+\frac{\beta}{\omega}\left(\frac{390}{\omega^2}-\frac{105}{8}\frac{\beta^2}{\omega^2}-5\right)\cos\omega t+\frac{\beta^2}{\omega^2}\left(\frac{5}{2}-\frac{15}{8}\frac{\beta^2}{\omega^2}+\frac{435}{4\omega^2}\right)\cos 2\omega t\\
&\quad-\frac{525}{8}\frac{\beta^2}{\omega^3}\sin 2\omega t-\frac{\beta^3}{\omega^3}\left(\frac{15}{8}+\frac{10}{\omega}\right)\sin 3\omega t-\frac{15}{64}\frac{\beta^4}{\omega^4}\cos 4\omega t.
\end{aligned}\right\} \tag{9.4}$$

Using these expressions, we have computed the unsteady separation profile up to quartic order and compared it with the actual time evolution of the fluid near the boundary. Advecting a thin layer of fluid particles in time, we have found that they indeed separate from the wall along the time-dependent separation profile predicted by our theory (figure 13). For comparison, we also show instantaneous streamlines in the figure, noting that the instantaneous streamline separation point (zero skin friction point) has no direct relationship to the true separation point. Also note that just as in the steady case (figure 1), flow separation starts with the formation of a tip away from the actual point of separation, with the true separation point and profile only prevailing later.

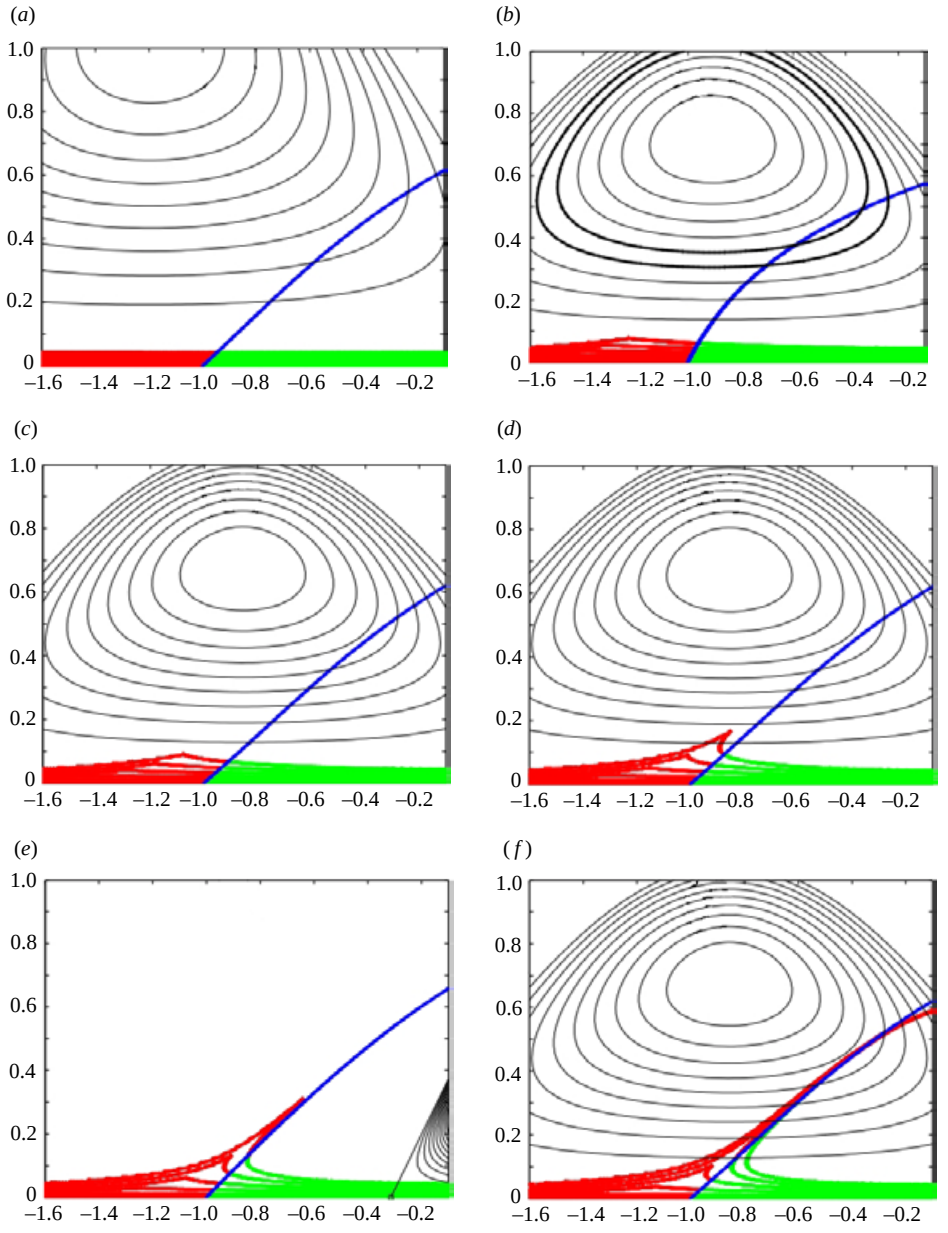

FIGURE 13. Separating fluid particles (green and red), the quartic separation profile predicted from our theory (blue), and instantaneous streamlines (black) in the time-periodic separation bubble model. The parameter values are $\omega = 2\pi$ and $\beta = 3$. Particles with different colours were released from different sides of the predicted separation profile at $t = 0$. The figures correspond to the times (*a*) $t = 0$, (*b*) $t = 8.2$, (*c*) $t = 9.95$, (*d*) $t = 15.0$, (*e*) $t = 18.65$, (*f*) $t = 25$.

We finally show how the moving separation formulae (8.3) and (8.6) also give the correct separation location and separation slope in this example. The sinusoidal time dependence here makes the mean operation $\langle \cdot \rangle$ straightforward to perform

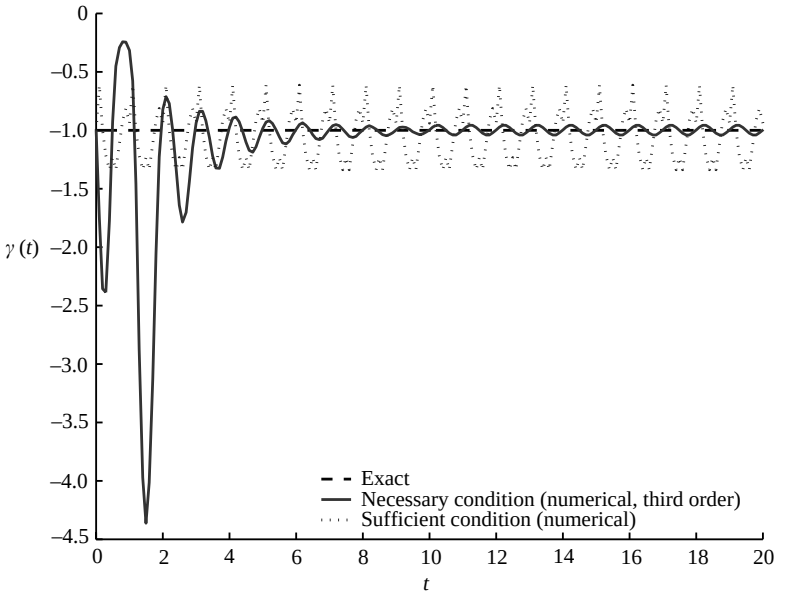

FIGURE 14. Separation point of the time-periodic separation bubble flow. The figure shows the exact location, as well as the location obtained from a numerical implementation of our necessary and sufficient moving separation criteria.

analytically:

$$\left\langle \int_{t_0}^{t_0-T} u_y(x,0,s)\,\mathrm{d}s \right\rangle = \left\langle \int_{t_0}^{t_0-T} (-1+x^2+\beta x \sin\omega s)\,\mathrm{d}s \right\rangle$$
$$= \left\langle (1-x^2)T + \frac{\beta x}{\omega}[\cos\omega t_0 - \cos\omega(t_0-T)] \right\rangle$$
$$= (1-x^2)T + \frac{\beta x}{\omega}\cos\omega t_0. \tag{9.5}$$

Thus, the moving separation criteria, (8.3), yield the separation conditions

$$1-\gamma^2(t_0)=0, \qquad -2\gamma(t_0)>0, \tag{9.6}$$

which give the exact fixed separation point $\gamma(t_0)\equiv -1$. Similarly, when evaluated, (8.6) reproduces the separation slope formula in (9.4).

We show in figure 14 how the numerical implementation of the necessary and the sufficient moving separation criteria perform on this example. We used a third-order polynomial least-squares fit to extract the mean component of (9.5) numerically. Because the exact mean is a linear function of T, our numerics produced a small oscillating error in the location of the separation point. This error decreases for higher-order polynomial fits, and for smaller step-sizes in the numerical integration.

9.2. *Compressible separation bubble*

To test our general separation criteria, we now add a phenomenological compressible term to the separation bubble velocity field. We let

$$\begin{aligned} u(x,y,t) &= -y+3y^2+x^2y-\tfrac{2}{3}y^3+\beta xy\sin\omega t,\\ v(x,y,t) &= -xy^2-\tfrac{1}{2}\beta y^2\sin\omega t+\mathrm{d}(t)y, \end{aligned} \tag{9.7}$$

where, for $T = 2\pi/\omega$,

$$\mathrm{d}(t) = \begin{cases} d_0, & t \bmod T \in [0, T/4], \\ -d_0/3, & t \bmod T \in (T/4, T). \end{cases} \tag{9.8}$$

We have selected a linear compressible term for simplicity. The function $\mathrm{d}(t)$ has mean zero to ensure bounded density and wall-tangential density gradients (cf. (6.14) and (6.15)). For this choice of $\mathrm{d}(t)$, our main physical assumptions (2.7) and (2.8) are satisfied.

Evaluating the density-independent versions of the necessary criteria (6.17) and (6.20), we find that

$$\left.\begin{aligned} \int_0^T \exp\left(\int_{t_0}^t v_y(\gamma, 0, s)\,\mathrm{d}s\right) u_y(\gamma, 0, t)\,\mathrm{d}t = 0, \\ \int_0^T \exp\left(\int_{t_0}^t v_y(\gamma, 0, s)\,\mathrm{d}s\right) v_{yy}(\gamma, 0, t)\,\mathrm{d}t > 0, \end{aligned}\right\} \tag{9.9}$$

must hold at the separation point for any choice of t_0. Computing these integrals, we obtain the separation point location

$$\gamma = -A - \sqrt{A^2 + 1} \quad \text{where} \quad A = \frac{d_0^2 \beta}{6\left(d_0^2 + \omega^2\right)\left(1 - \exp(-d_0 T/4)\right)}. \tag{9.10}$$

This formula gives a separation point that differs from the zero-mean-skin-friction point $x = -1$ for non-zero values of the compressibility parameter d_0, even though the velocity field is time-periodic.

To obtain a linear approximation for the unsteady separation profile, we use the formulation of § 2.7 to rewrite the separation slope formula (6.22) as

$$f_0(t_0) = \frac{\displaystyle\int_0^T \left[a_y(t) \exp\left(2\int_{t_0}^t v_y(\gamma, 0, s)\,\mathrm{d}s\right) - 3 b_y(t) \exp\left(\int_{t_0}^t v_y(\gamma, 0, s)\,\mathrm{d}s\right) \times \int_{t_0}^t a(s) \exp\left(\int_{t_0}^s v_y(\gamma, 0, r)\,\mathrm{d}r\right)\mathrm{d}s\right]\mathrm{d}t}{\displaystyle 3\int_0^T b_y(t) \exp\left(\int_{t_0}^t v_y(\gamma, 0, s)\,\mathrm{d}s\right)\mathrm{d}t}, \tag{9.11}$$

with a, a_y and b_y being the same as in the incompressible limit considered in the previous section. In our simulation described below, we evaluated $f_0(t_0)$ numerically to obtain a prediction for the instantaneous separation angle.

Advecting a layer of fluid particles, we have again found that the flow indeed separates from the wall at the predicted separation point (9.10) (figure 15). The separation point is not the zero mean-skin-friction point despite the exact time-periodicity of the flow. This agrees with the conclusions of Yuster & Hackborn (1997), who showed that the results of Shariff *et al.* (1991) are inapplicable to compressible time-periodic flows.

9.3. *Unstable separation bubble*

Both flows we have considered so far have been time-periodic and exhibited fixed unsteady separation. We now turn to a version of the separation bubble flow that exhibits aperiodic time dependence and produces moving unsteady separation.

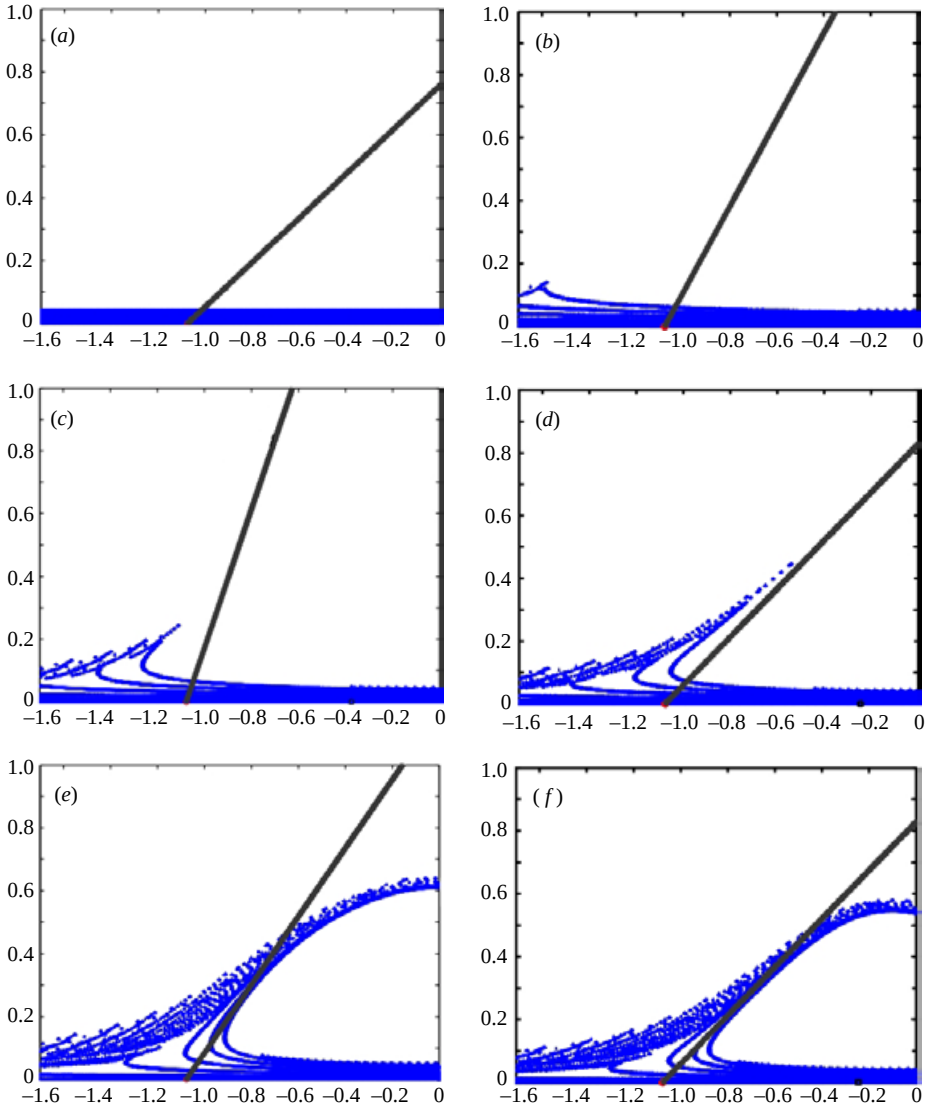

FIGURE 15. Linear prediction for the separation profile and actual flow separation in the compressible oscillating separation bubble model with $\omega = 1$, $\beta = 3$ and $d_0 = 1$. The small square on the wall denotes the instantaneous skin friction point (when in range), and the small circle denotes the true separation point. Particle positions are shown at (*a*) $t = 0$, (*b*) $t = 7.15$, (*c*) $t = 10.45$, (*d*) $t = 12.65$, (*e*) $t = 23.10$, (*f*) $t = 23.65$.

For high Reynolds numbers, steady flows with stagnation points tend to be unstable, with oscillatory instabilities growing exponentially in time (Friedlander & Vishik 1991; Lifshitz 1991). As a consequence, small perturbations of a steady separation bubble will lead to exponentially growing oscillations of the bubble for large enough Reynolds numbers. To model a case where these growing oscillations saturate over time, we consider the incompressible velocity field

$$\left.\begin{aligned} u(x, y, t) &= -y + 3y^2 + x^2 y - \tfrac{2}{3}y^3 + \beta(1 - e^{-\alpha t})xy \sin^2 \omega t, \\ v(x, y, t) &= -xy^2 - \tfrac{1}{2}\beta(1 - e^{-\alpha t})2y^2 \sin^2 \omega t, \end{aligned}\right\} \tag{9.12}$$

where $\alpha > 0$ is a parameter controlling the strength of the instability.

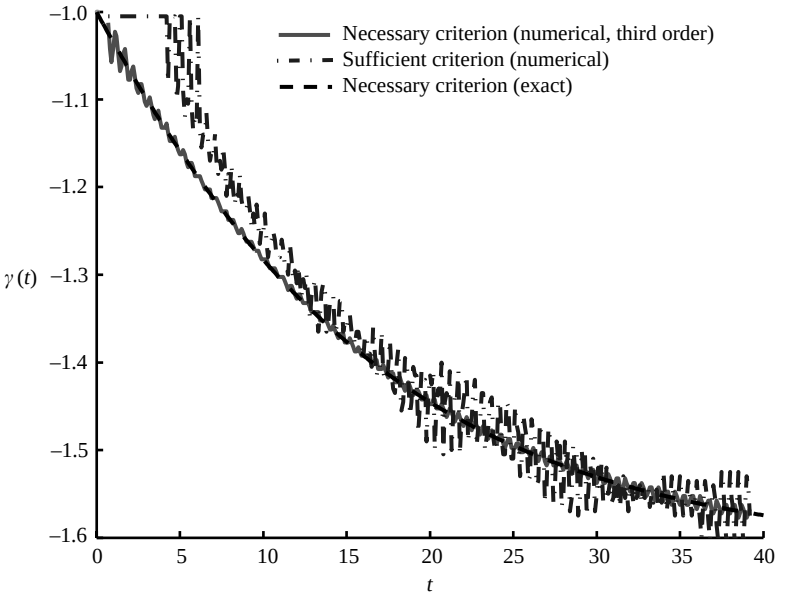

FIGURE 16. Moving separation location for the unstable separation bubble model.

To evaluate the necessary conditions for moving separation, we note that

$$\int_{t_0}^{t_0-T} u_y(x,0,s)\,\mathrm{d}s = \int_{t_0}^{t_0-T} \left[x^2 - 1 + \tfrac{1}{2}\beta x(1-e^{-\alpha s})(1-\cos 2\omega s)\right]\mathrm{d}s, \tag{9.13}$$

and hence

$$\left\langle \int_{t_0}^{t_0-T} u_y(x,0,s)\,\mathrm{d}s \right\rangle = -(x^2 - 1 + \beta x/2)T + \frac{\beta x}{4\omega}\sin 2\omega t_0 + \frac{\beta x}{2\alpha}(\exp(-\alpha(t_0-T)) - \exp(-\alpha t_0)). \tag{9.14}$$

Then the moving separation conditions (8.3) yield

$$\gamma^2(t_0) + \tfrac{1}{2}\beta\gamma(t_0)(1-\exp(-\alpha t_0)) - 1 = 0, \qquad -2\gamma(t_0) + \tfrac{1}{2}\beta(\exp(-\alpha t_0) - 1) > 0, \tag{9.15}$$

giving the exact moving separation location

$$\gamma(t_0) = \tfrac{1}{4}\beta(\exp(-\alpha t_0) - 1) - \sqrt{\tfrac{1}{16}\beta^2(\exp(-\alpha t_0) - 1)^2 + 1}, \tag{9.16}$$

plotted with a dashed line in figure 16.

Using the two procedures described in § 8, we also locate the moving separation point numerically. Figure 16 shows the results from the heuristic necessary and the analytic sufficient criteria of § 8. For the necessary criterion, we used a third-order polynomial least-squares fit to identify the mean component of $\int_{t_0}^{t_0-T} u_y(x,0,s)\,\mathrm{d}s$; we then located $x = \gamma(t_0)$, the point at which the coefficient of the linear polynomial term changed sign (see (8.3)).

For the sufficient moving separation criterion, we determined $T_m(t_0)$ as the solution of (8.11). (For times $t \in [0, 40.00]$, the integration times $T_m(t)$ are shown in figure 17). With $T_m(t_0)$ at hand, we plotted the effective separation point $\gamma_{eff}(T_m(t_0), t_0)$ (the location of a finite-time unstable manifold) in figure 16.

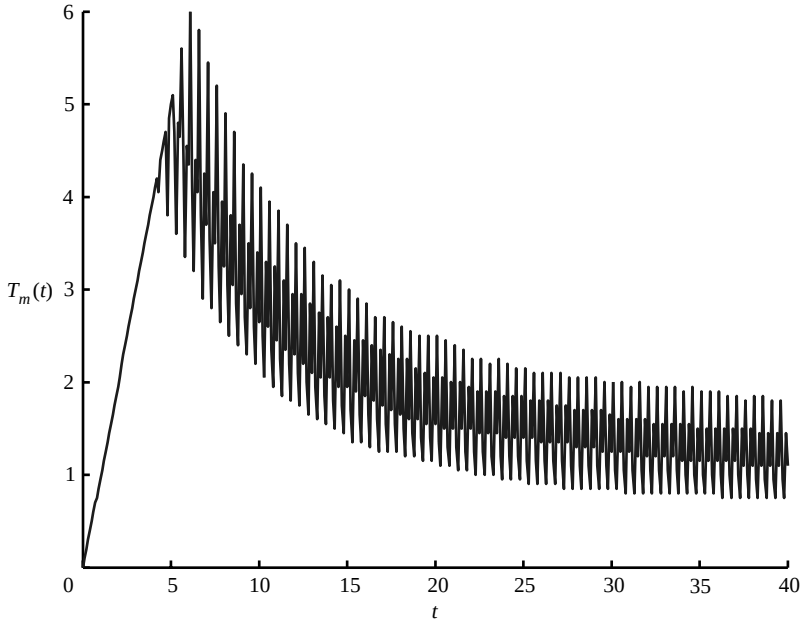

FIGURE 17. Moving separation time scale as a function of the present time for the unstable separation bubble model. The parameter values are $\beta = 2$, $\alpha = 0.007$ and $\omega = 2\pi$. (We plot t_0 itself whenever $t_0 - T_m(t_0)$ would be negative.)

The separation points obtained from the two numerical methods typically differ from the exact location in (9.16), but after initial transients, both criteria track the actual moving separation point closely. As we indicated earlier, the necessary criterion produces a point that actually converges to the exact moving separation point as more and more past velocity data are used in calculating $\int_{t_0}^{t_0-T} u_y(x, 0, s)\,\mathrm{d}s$.

We show the results of a particle simulation with the computed linear separation profiles superimposed in figure 18. For the heuristic necessary criterion, we used (8.6) to compute the separation slope, employing a fourth-order polynomial least-squares fit in extracting the mean components. For the analytic sufficient criterion, we used (8.14) to obtain the separation slope. As already suggested by figure 16, we obtain virtually identical linear separation profiles from both moving separation algorithms if t_0 is large enough.

9.4. *Randomly oscillating separation bubble*

Consider the velocity field

$$\left.\begin{aligned} u(x, y, t) &= -y + 3y^2 + x^2 y - \tfrac{2}{3}y^3 + \beta xy[A\log(t + B) + r(t)], \\ v(x, y, t) &= -xy^2 - \tfrac{1}{2}\beta y^2[A\log(t + B) + r(t)], \end{aligned}\right\} \tag{9.17}$$

where $\beta, A, B > 0$ are parameters, and $r(t)$ is a mean-zero random variable of normal distribution. This velocity field models a growing separation bubble with a well-defined mean growth, onto which substantial random oscillations are superimposed.

We now have

$$\int_{t_0}^{t_0-T} u_y(x, 0, s)\,\mathrm{d}s = \int_{t_0}^{t_0-T} [x^2 - 1 + \beta x[A\log(s + B) + r(s)]]\,\mathrm{d}s, \tag{9.18}$$

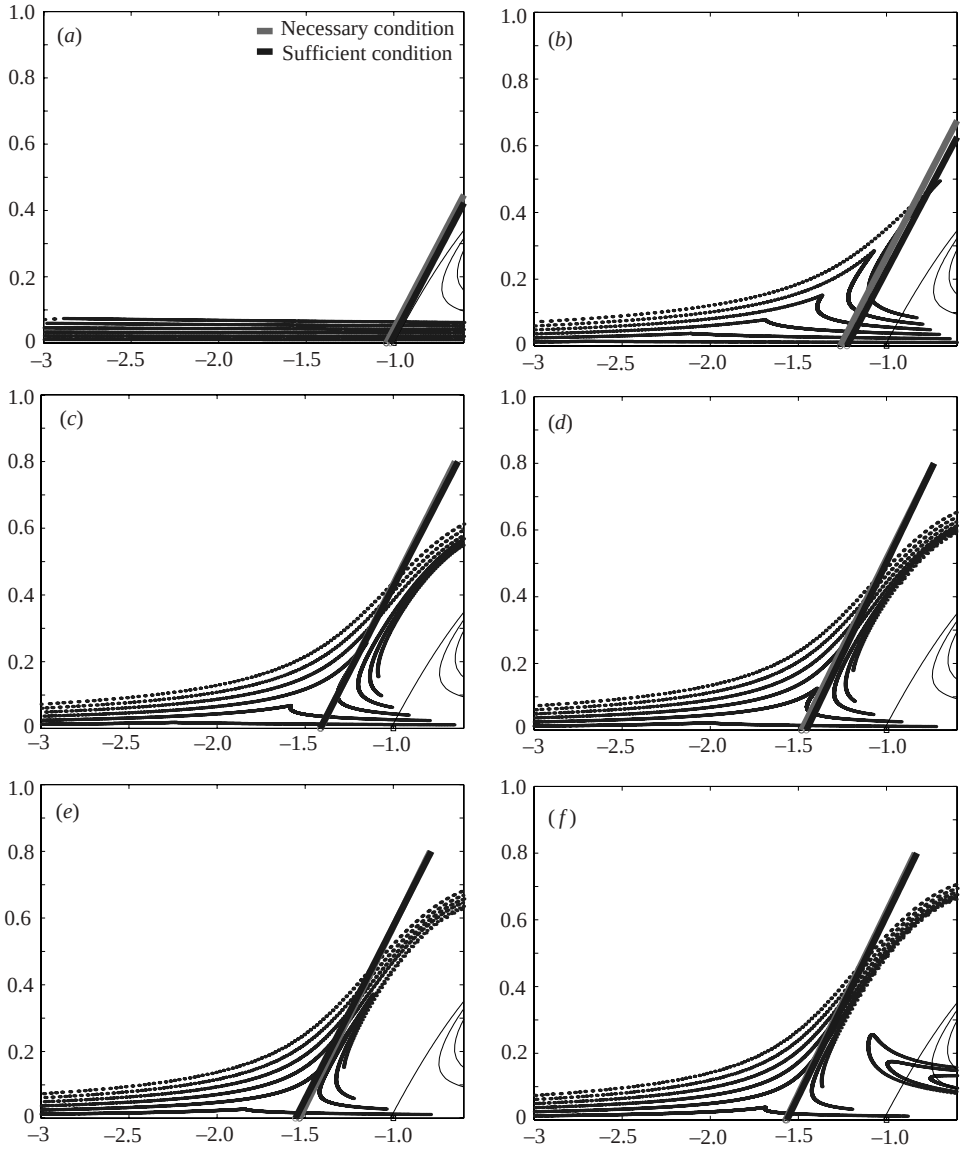

FIGURE 18. Flow separation in the unstable separation bubble model: separating fluid particles, instantaneous streamlines, linear separation profile computed from the necessary criterion (light thick line), and linear separation profile computed from the sufficient criterion (dark thick line). The figure correspond to times (*a*) $t = 1$, (*b*) $t = 9$, (*c*) $t = 17$, (*d*) $t = 23$, (*e*) $t = 29$, (*f*) $t = 37$.

and hence

$$\left\langle \int_{t_0}^{t_0-T} u_y(x,0,s)\,\mathrm{d}s \right\rangle = (1-x^2)T + \beta A x[(t_0 - T + B)\log(t_0 - T + B) + T] - \beta A x(t_0 + B)\log(t_0 + B) + \beta x \int_{t_0}^{t_0-T} r(s)\,\mathrm{d}s. \quad (9.19)$$

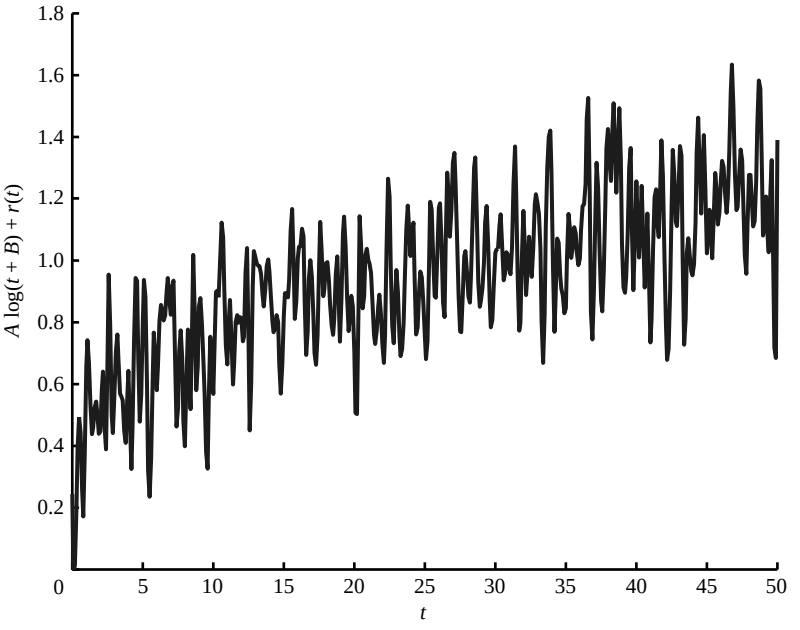

FIGURE 19. Typical time-dependence for the random velocity field.

Because $r(t)$ has zero mean, its integral converges to zero for increasing T. Thus, in a statistical sense, the necessary separation criteria (8.3) yield the conditions

$$\gamma^2(t_0) - \beta A[\log(t_0 + B)]\gamma(t_0) - 1 = 0, \qquad -2\gamma(t_0) - \beta A \log(t_0 + B) > 0, \tag{9.20}$$

giving the *statistically exact* moving separation location

$$\gamma(t_0) = -\tfrac{1}{2}\beta A \log(t_0 + B) - \sqrt{\tfrac{1}{4}\beta^2 A^2 \log^2(t_0 + B) + 1}. \tag{9.21}$$

This is the moving separation location at time $t = t_0$ observed on the average over many realizations of $r(t)$.

The exact separation location in a given realization of $r(t)$ will differ from (9.21), and can only be identified numerically. In our test simulation, we selected $\beta = 4$, $A = 0.3$ and $B = 3$, and set the standard deviation of $r(t)$ equal to 0.2. We sampled $r(t)$ at multiples of $\Delta t = 0.2$, and used a cubic spline interpolation to obtain velocity values in (9.17) for intermediate times. With these parameters, a particular realization of the random velocity field coefficient $A \log(t + B) + r(t)$ is shown in figure 19.

In figure 20, we show the statistically exact separation point along with those obtained numerically from the necessary and the sufficient moving separation criteria. (The integration time scale $T_m(t)$ obtained from the sufficient criterion (8.11) is shown in figure 21.)

Figure 20 shows that both the necessary and the sufficient conditions track the rough location of the statistically exact mean separation location. The analytic sufficient criterion, however, outperforms the heuristic necessary condition in accuracy, as seen in the snapshots of figure 22. (For a full animation, see web.mit.edu/ghaller/www/2dseparation.html.)

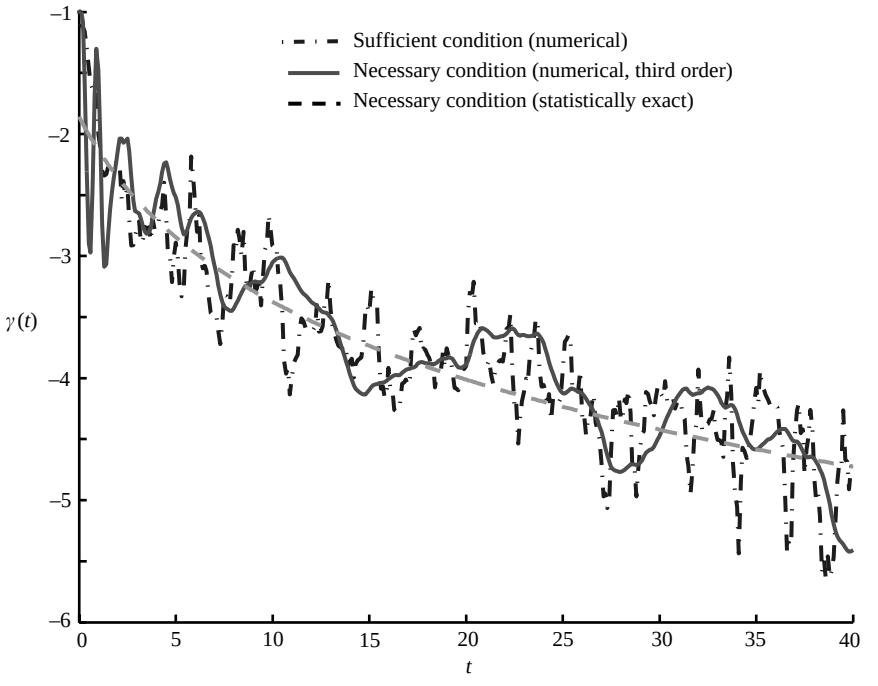

FIGURE 20. Moving separation location in the randomly oscillating separation bubble model.

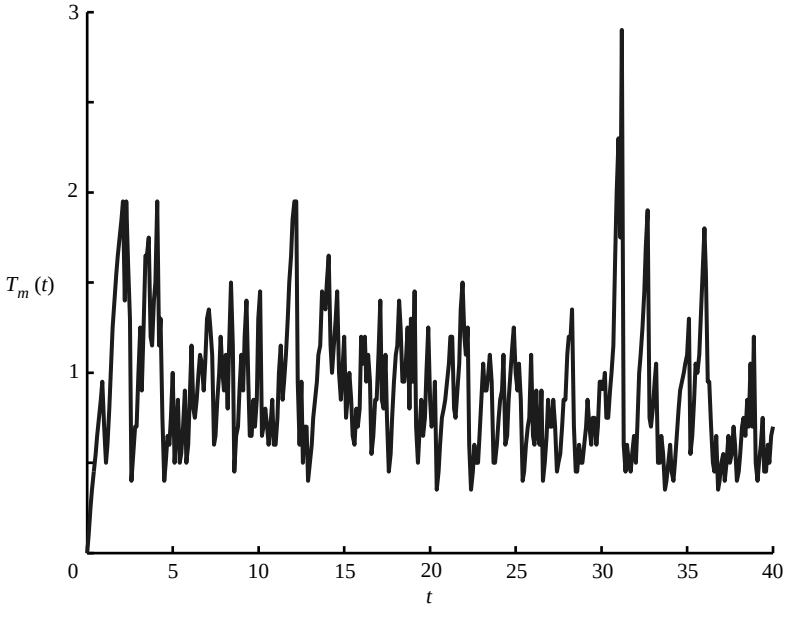

FIGURE 21. Moving separation time scale as a function of the present time for the randomly oscillating separation bubble model. (We plot t_0 itself whenever $t_0 - T_m(t_0)$ would be negative.)

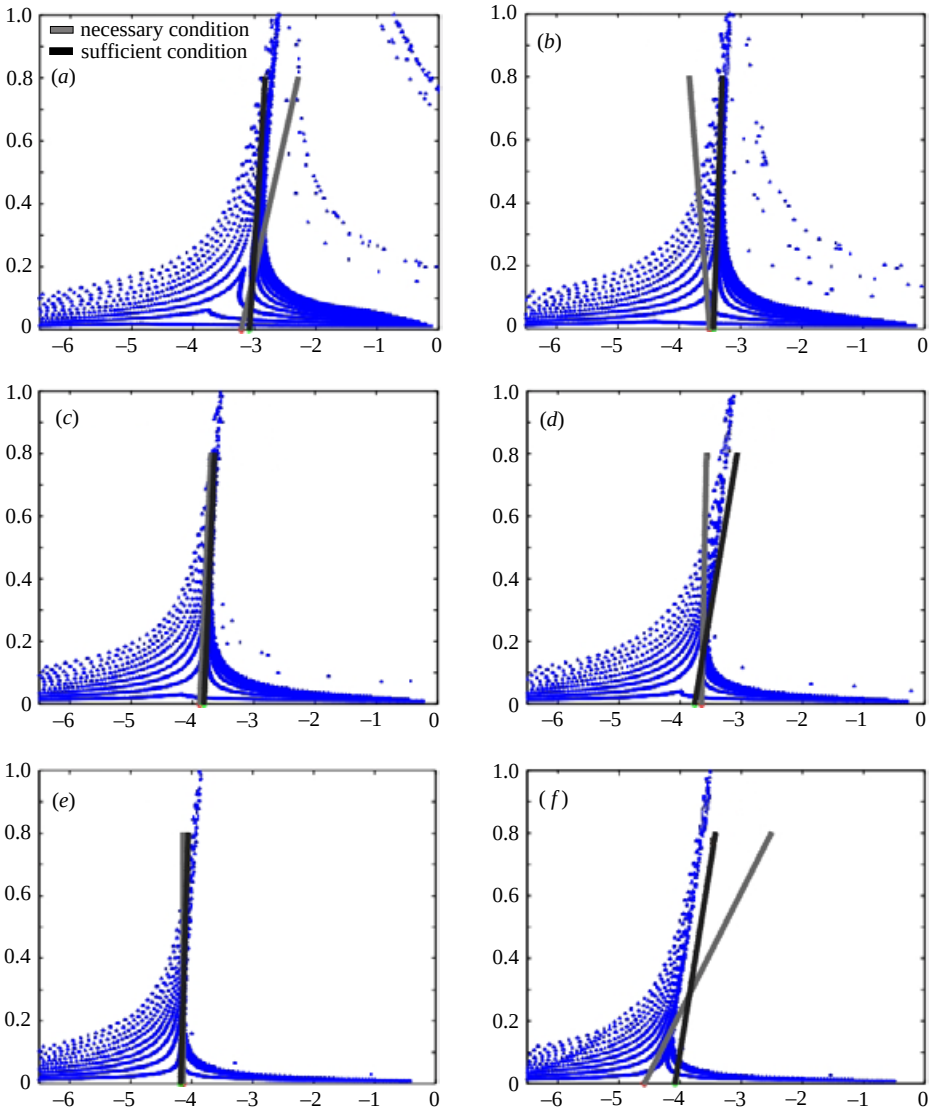

FIGURE 22. Flow separation in the randomly oscillating separation bubble model: separating fluid particles, linear separation profile computed from the heuristic necessary criterion (light thick line), and linear separation profile computed from the analytic sufficient criterion (dark thick line). The figure correspond to times (*a*) $t=9$, (*b*) $t=13$, (*c*) $t=18$, (*d*) $t=22$, (*e*) $t=31$, (*f*) $t=35$.

10. Conclusions

We have developed a rigorous theory of two-dimensional unsteady separation that relates the formation of a material spike near a no-slip boundary to the existence of an unstable manifold for a distinguished point on the boundary. This theory is frame-independent, and only assumes regularity and mass conservation along the boundary. In particular, the velocity field does not have to solve the boundary-layer equations or the Navier–Stokes equations: it can be an arbitrary numerical, experimental, or model field.

The existence of a wall-bound unstable manifold (separation profile) is guaranteed by Prandtl's classic separation criteria for steady flows with no-slip boundaries. Here, we have extended these criteria to unsteady compressible flows with general time dependence, covering separation and reattachment on fixed and moving boundaries. We have also given an algorithm for computing the shape of the unstable manifold via a Taylor expansion. This expansion becomes particularly simple for incompressible flows, for which we have obtained a quartic approximation of the separation profile.

We have also given a theoretical description of moving separation using finite-time invariant manifolds. The two algorithms we described in § 8.1 locate moving separation and reattachment profiles in incompressible flows with general aperiodic time dependence. As we illustrated in examples, these algorithms are to be used if the fixed or moving nature of separation is *a priori* unknown.

While motivated by Lagrangian arguments, our criteria are fully Eulerian, and hence do not require the advection of fluid particles. In addition, these criteria only use quantities computed from distributed pressure and skin-friction measurements along the wall (cf. § 4), and hence are applicable in active flow control.

Being purely kinematic, our analysis does not distinguish between laminar and turbulent separation. Further work is required, however, on the computational difficulties in moving turbulent separation. These difficulties arise from errors in the long-term numerical integration of our criteria, and from errors in identifying the mean component of the backward-time skin-friction integral.

The no-slip assumption (2.2) on the boundary is crucial in our theory, thus compressible fluids with slip boundary conditions are not covered by the present results. The case of slip boundaries is actually simpler to analyse, because we can use the classic theory of hyperbolic invariant manifolds to describe separation profiles (see Wang *et al.* 2003).

Beyond the further testing of our results on numerical and experimental velocity data, a notable challenge is the extension of the theory to three-dimensional unsteady flows. The Lagrangian definition of separation extends to three dimensions, but technical difficulties arise in the derivation of Eulerian criteria for fixed and moving unstable manifolds. Some of these difficulties are related to the increased dimensionality of the problem, whereas others are related to the variety of topologically different separation profiles that a three-dimensional unsteady flow may support. We are addressing these challenges in ongoing work (Grunberg, Surana & Haller 2004).

This work was supported by AFOSR Grant F49620-03-1-0200, and NSF Grant DMS-98-00922. I would like to thank Avi Seifert, Lex Smits, Yong Wang and the anonymous referees for their remarks. I am also grateful to Mohammed-Reza Alam, Olivier Grunberg, Weijiu Liu, Pan Mao and Amit Surana for their close reading of the manuscript, and for all the improvements they suggested. Hayder Salman's numerical observations and his suggestion of considering the kinematic separation model of Ghosh *et al.* (1998) were very helpful in developing the ideas of this paper.

Appendix A

After substituting formula (2.20) for $f(\tau)$ in (2.29), we obtain

$$f_1(t) = \frac{f_1(t_0)\rho^2(t)}{\rho^2(t_0)} + \rho^2(t)\int_{t_0}^{t}\left[P(\tau,t_0) + f_0(t_0)Q(\tau,t_0,t) - \frac{f_0^2(t_0)b_x(\tau)}{\rho^2(t_0)}\right]\mathrm{d}\tau, \quad \text{(A 1)}$$

where

$$P(\tau,t_0)=\frac{a_y(\tau)}{\rho^2(\tau)}+\frac{a_x(\tau)-b_y(\tau)}{\rho(\tau)}\int_{t_0}^{\tau}\frac{a(s)}{\rho(s)}\,\mathrm{d}s-b_x(\tau)\left(\int_{t_0}^{\tau}\frac{a(s)}{\rho(s)}\,\mathrm{d}s\right)^2,$$
$$Q(\tau,t_0,t)=\frac{1}{\rho(t_0)}\left[\frac{a_x(\tau)-b_y(\tau)}{\rho(\tau)}-2b_x(\tau)\int_{t_0}^{\tau}\frac{a(s)}{\rho(s)}\,\mathrm{d}s\right]. \tag{A 2}$$

We first observe that for material lines emanating from the separation point $(\gamma,0)$ with slopes larger or smaller than the slope of the separation profile, $f_1(t)$ will tend to plus or minus infinity, respectively, as $t\to-\infty$. This is because in backward time, the separation profile – as any unstable manifold – also repels material lines that emanate from the separation point, but do not coincide with the separation profile.

As a consequence, for any $\varepsilon\neq 0$, (A 1) yields

$$\int_{t_0}^{-\infty}\left[P(\tau,t_0)+[f_0(t_0)+\varepsilon]Q(\tau,t_0,t)-\frac{[f_0(t_0)+\varepsilon]^2b_x(\tau)}{\rho^2(t_0)}\right]\mathrm{d}\tau=\text{sign }(\varepsilon)\infty. \tag{A 3}$$

On the separation profile itself, however, $f_1(t)$ remains bounded, i.e.

$$\limsup_{t\to-\infty}\left|\int_{t_0}^{t}\left[P(\tau,t_0)+f_0(t_0)Q(\tau,t_0,t)-\frac{f_0^2(t_0)b_x(\tau)}{\rho^2(t_0)}\right]\mathrm{d}\tau\right|<\infty. \tag{A 4}$$

Comparing these two expressions we obtain

$$\int_{t_0}^{-\infty}\left[Q(\tau,t_0,t)-[2f(_0t_0)+\varepsilon]\frac{b_x(\tau)}{\rho^2(t_0)}\right]\mathrm{d}\tau=\infty. \tag{A 5}$$

By assumptions (2.7)–(2.8), we can write

$$\limsup_{t\to-\infty}\left|\int_{t_0}^{t}[2f_0(t_0)+\varepsilon]\frac{b_x(\tau)}{\rho^2(t_0)}\,\mathrm{d}\tau\right|=\frac{|2f_0(t_0)+\varepsilon|}{\rho^2(t_0)}\limsup_{t\to-\infty}\left|\int_{t_0}^{t}v_{xy}(\gamma,0,\tau)\,\mathrm{d}\tau\right|<\infty, \tag{A 6}$$

therefore (A 5) simplifies to

$$\int_{t_0}^{-\infty}Q(\tau,t_0,t)\,\mathrm{d}\tau=\infty, \tag{A 7}$$

or equivalently,

$$\int_{t_0}^{-\infty}\left[\frac{a_x(\tau)-b_y(\tau)}{\rho(\tau)}-2b_x(\tau)\int_{t_0}^{\tau}\frac{a(s)}{\rho(s)}\,\mathrm{d}s\right]\mathrm{d}\tau=\infty, \tag{A 8}$$

as claimed in the necessary separation condition (2.22).

To prove (2.30), observe that (A 6) simplifies the boundedness condition (A 4) to

$$\limsup_{t\to-\infty}\left|\int_{t_0}^{t}[P(\tau,t_0)+f_0(t_0)Q(\tau,t_0,t)]\,\mathrm{d}\tau\right|<\infty, \tag{A 9}$$

which, together with (A 7), implies

$$\lim_{t\to-\infty}\frac{\displaystyle\int_{t_0}^{t}[P(\tau,t_0)+f_0(t_0)Q(\tau,t_0,t)]\,\mathrm{d}\tau}{\displaystyle\int_{t_0}^{t}Q(\tau,t_0,t)\,\mathrm{d}\tau}=0. \tag{A 10}$$

However, this is equivalent to

$$f_0(t_0) = -\lim_{t\to-\infty} \frac{\displaystyle\int_{t_0}^{t} P(\tau, t_0)\,\mathrm{d}\tau}{\displaystyle\int_{t_0}^{t} Q(\tau, t_0, t)\,\mathrm{d}\tau}, \tag{A 11}$$

which is in turn equivalent to (2.30).

Appendix B

Computing the $O(y, y^2, y^3)$ terms in the incompressible separation equation (3.8) leads to the set of equations

$$\dot{f}_1 = (a_x - c) f_0 + a_y, \tag{B 1}$$

$$\dot{f}_2 = a_{yy} + 2[a_{xy} - c_y] f_0 + [a_{xx} - 2c_x] f_0^2 + 2[a_x - 2c] f_1, \tag{B 2}$$

$$\begin{aligned}\dot{f}_3 = {} & a_{yyy} + (a_{xxx} - 3c_{xx}) f_0^3 + 3(a_{xxy} - 2c_{xy}) f_0^2 + 3(a_{xyy} - c_{yy}) f_0 \\ & + 6(a_{xx} - 3c_x) f_0 f_1 + 6(a_{xy} - 2c_y) f_1 + 3(a_x - 3c) f_2,\end{aligned} \tag{B 3}$$

$$\begin{aligned}\dot{f}_4 = {} & a_{yyyy} + (a_{xxxx} - 4c_{xxx}) f_0^4 + 4(a_{xxxy} - 3c_{xxy}) f_0^3 + 6(a_{xxyy} - 2c_{xyy}) f_0^2 \\ & + 4(a_{xyyy} - c_{yyy}) f_0 + 12(a_{xxx} - 4c_{xx}) f_0^2 f_1 + 24(a_{xxy} - 3c_{xy}) f_0^2 f_1 \\ & + 12(a_{xyy} - 2c_{yy}) f_1 + 12(a_{xx} - 4c_x) f_1^2 + 12(a_{xx} - 4c_x) f_0 f_2 \\ & + 12(a_{xy} - 3c_y) f_2 + 4(a_x - 4c) f_3.\end{aligned} \tag{B 4}$$

We note the following incompressibility relations derived from (3.6):

$$a_x + 2c = 0, \quad a_{xy} + 3c_y = 0, \quad a_{xx} + 2c_x = 0, \tag{B 5a–c}$$

$$a_{xxx} + 2c_{xx} = 0, \quad a_{xxy} + 3c_{xy} = 0, \quad a_{xyy} + 4c_{yy} = 0, \tag{B 5d–f}$$

$$a_{xxxx} + 2c_{xxx} = 0, \quad a_{xxxy} + 3c_{xxy} = 0, \tag{B 5g,h}$$

$$a_{xxyy} + 4c_{xyy} = 0, \quad a_{xyyy} + 5c_{yyy} = 0. \tag{B 5i,j}$$

We first integrate (B 1), then substitute (3.10) and use (B 5*a*) to obtain

$$f_1(t) = f_1(t_0) + \int_{t_0}^{t} \left[a_y(\tau) - 3c(\tau) f_0(t_0) - 3c(\tau) \int_{t_0}^{\tau} a(s)\,\mathrm{d}s \right] \mathrm{d}\tau \tag{B 6}$$

for the first-order term in the expansion for the incompressible separation profile. Because $f_1(t)$ remains bounded in backward time at a fixed separation point, we can use the argument of Appendix A to derive (3.16) from (B 6). The expression (3.16) can also be obtained by setting $b(\tau) \equiv 0$ and $b_y(\tau) = c(\tau)$ in its compressible counterpart (2.30).

Next we integrate (B 2) and observe that the boundedness of $f_2(t)$ implies the boundedness of the integral

$$\int_{t_0}^{t} \left[a_{yy}(\tau) - 8c_y(\tau) f_0(\tau) - 4c_x(\tau) f_0^2(\tau) - 8c(\tau) f_1(\tau) \right] \mathrm{d}\tau \tag{B 7}$$

for all $t \leqslant t_0$. Invoking the arguments of Appendix A, then substituting (B 6) and using (B 5) leads to (3.17). Again, this result also follows from the compressible curvature formula (2.33) if we note that

$$b = 0, \quad b_x = 0, \quad b_y = c, \quad b_{xx} = 0, \quad b_{xy} = c_x, \quad b_{yy} = c_y, \tag{B 8}$$

hold for incompressible flows.

We now integrate (B 3) and use the incompressibility conditions in (B 5) to find that the integral

$$\int_{t_0}^{t} \left[a_{yyy} - 5c_{xx} f_0^3 - 15c_{xy} f_0^2 - 15c_{yy} f_0 - 30c_y f_1 - 30c_x\, f_0 f_1 - 15c f_2\right] \mathrm{d}\tau \qquad \text{(B 9)}$$

must be bounded for all $t \leqslant t_0$. Proceeding again as above, we use this boundedness to obtain (3.18). Finally, we integrate (B 4) and follow the same procedure to obtain the last formula in (3.19).

Appendix C

Recall that the flow map associated with (2.1) is defined as

$$\boldsymbol{F}_{t_0}^{t}(x_0, y_0) = \begin{pmatrix} x(t; x_0, y_0, t_0) \\ y(t; x_0, y_0, t_0) \end{pmatrix}. \qquad \text{(C 1)}$$

The Jacobian of this map, usually called the deformation gradient, is given by the formula

$$\nabla \boldsymbol{F}_{t_0}^{t}(x_0, y_0) = \begin{pmatrix} \dfrac{\partial x(t)}{\partial x_0} & \dfrac{\partial x(t)}{\partial y_0} \\ \dfrac{\partial y(t)}{\partial x_0} & \dfrac{\partial y(t)}{\partial y_0} \end{pmatrix}. \qquad \text{(C 2)}$$

If u and v are continuously differentiable, then the entries of the matrix $\nabla \boldsymbol{F}_{t_0}^{t}$ remain bounded on bounded domains for any finite t (cf. Arnold 1978). In view of this, the formula

$$\det \nabla \boldsymbol{F}_{t_0}^{t} = \frac{\partial x(t)}{\partial x_0}\frac{\partial y(t)}{\partial y_0} - \frac{\partial x(t)}{\partial y_0}\frac{\partial y(t)}{\partial x_0} \qquad \text{(C 3)}$$

and Van Dommelen's condition (2.39) together imply

$$\det \nabla \boldsymbol{F}_{t_0}^{t}(\gamma, \eta) = 0. \qquad \text{(C 4)}$$

This last equation, however, contradicts Liouville's formula

$$\det \nabla \boldsymbol{F}_{t_0}^{t}(\gamma, \eta) = \exp\left(\int_{t_0}^{t} \nabla \cdot \boldsymbol{v}(x(s; \gamma, \eta, t_0), y(s; \gamma, \eta, t_0), s)\, \mathrm{d}s\right), \qquad \text{(C 5)}$$

for continuously differentiable velocity fields (cf. Arnold 1978). Therefore, $\boldsymbol{v} = (u, v)$ cannot be continuously differentiable.

To find an exact Lagrangian criterion for fixed unsteady separation at a boundary point, we differentiate (2.1) with respect to the initial positions (x_0, y_0) to obtain the matrix differential equation

$$\frac{\mathrm{d}}{\mathrm{d}t}\nabla \boldsymbol{F}_{t_0}^{t}(x_0, y_0) = \begin{pmatrix} u_x\left(\boldsymbol{F}_{t_0}^{t}(x_0, y_0), t\right) & u_y\left(\boldsymbol{F}_{t_0}^{t}(x_0, y_0), t\right) \\ v_x\left(\boldsymbol{F}_{t_0}^{t}(x_0, y_0), t\right) & v_y\left(\boldsymbol{F}_{t_0}^{t}(x_0, y_0), t\right) \end{pmatrix} \nabla \boldsymbol{F}_{t_0}^{t}(x_0, y_0), \qquad \text{(C 6)}$$

with the initial condition

$$\nabla \boldsymbol{F}_{t_0}^{t}(x_0, y_0) = \begin{pmatrix} 1 & 0 \\ 0 & 1 \end{pmatrix}. \qquad \text{(C 7)}$$

Because of the no-slip boundary conditions, we have $u_x(x,0,t)=v_x(x,0,t)=0$; thus along the boundary, (C 6) simplifies to

$$\frac{\mathrm{d}}{\mathrm{d}t}\nabla \boldsymbol{F}_{t_0}^{t}(x_0,0)=\begin{pmatrix}0 & u_y\left(\boldsymbol{F}_{t_0}^{t}(x_0,0),t\right)\\ 0 & v_y\left(\boldsymbol{F}_{t_0}^{t}(x_0,0),t\right)\end{pmatrix}\nabla \boldsymbol{F}_{t_0}^{t}(x_0,0). \tag{C 8}$$

We solve this equation by direct integration, then use the density relation (2.5) and the initial condition (C 7) to obtain

$$\nabla \boldsymbol{F}_{t_0}^{t}(x_0,0)=\begin{pmatrix}1 & \rho(x_0,0,t_0)\displaystyle\int_{t_0}^{t}\frac{u_y(x_0,0,\tau)}{\rho(x_0,0,\tau)}\,\mathrm{d}\tau\\ 0 & \dfrac{\rho(x_0,0,t_0)}{\rho(x_0,0,t)}\end{pmatrix}. \tag{C 9}$$

Comparing this last expression with (C 2) gives

$$\left.\begin{aligned}\frac{\partial x(t;x_0,0,t_0)}{\partial x_0}&=1, \quad \frac{\partial x(t;x_0,0,t_0)}{\partial y_0}=\rho(x,0,t_0)\int_{t_0}^{t}\frac{u_y(x_0,0,\tau)}{\rho(x_0,0,\tau)}\,\mathrm{d}\tau,\\ \frac{\partial y(t;x_0,0,t_0)}{\partial x_0}&=0, \quad \frac{\partial y(t;x_0,0,t_0)}{\partial y_0}=\frac{\rho(x_0,0,t_0)}{\rho(x_0,0,t)},\end{aligned}\right\} \tag{C 10}$$

for any boundary point $(x_0,0)$. Therefore, by the necessary condition (2.21), if $x_0=\gamma$ is a separation point on the boundary, then necessarily

$$\limsup_{t\to-\infty}\left|\frac{\partial x(t;\gamma,0,t_0)}{\partial y_0}\right|<\infty. \tag{C 11}$$

As (C 10) shows, the remaining three elements of the deformation gradient show no special behaviour at separation points.

Appendix D

Here we prove a sufficient criterion for fixed sharp separation in incompressible flows under conditions (5.1) and (5.2). Beyond these two conditions, we assume that the velocity field as well as its first and second derivatives remain uniformly bounded for all times at the separation point. We will establish the existence of a unique material line that acts as an unstable manifold for the separation point $(\gamma,0)$.

We start by fixing γ and introducing the time-dependent coordinate change

$$q=x-\gamma-y\left(f_0(t)+yf_1(t)\right), \tag{D 1}$$

with $f_0(t)$ and $f_1(t)$ satisfying (3.10) and (B 6). Note that this change of coordinates transforms the $x=\gamma$ coordinate axis into the new $q=0$ axis that has a quadratic tangency with the candidate unstable manifold (separation profile) for all times. We obtain

$$\left.\begin{aligned}\dot q&=\dot x-\dot y f_0-y\dot f_0-2y\dot y f_1-y^2\dot f_1\\ &=yqa_x(t)+m_1(q,y,f_k,t)y^3+m_2(q,y,f_k,t)yq^2+m_3(q,y,f_k,t)y^2q,\\ \dot y&=y^2C(\gamma+yf_0+y^2f_1+q,y,t)\\ &=y^2\left[c(t)+ym_4(q,y,f_k,t)+qm_5(q,y,f_k,t)\right],\end{aligned}\right\} \tag{D 2}$$

as new equations of motion for fluid particles, with appropriate smooth functions m_i, and with f_k referring to f_0 and f_1. The $O(y)$ and $O(y^2)$ terms in the $\dot q$ equation

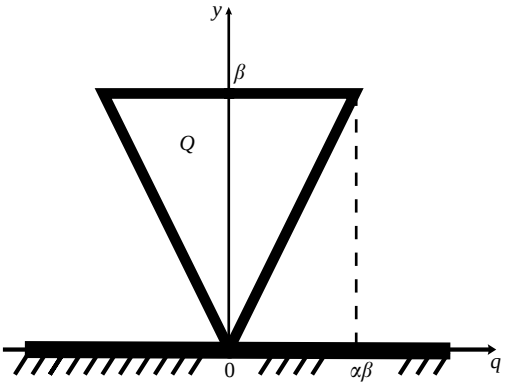

FIGURE 23. The definition of the cone Q.

vanish precisely because we chose $f_0(t)$ and $f_1(t)$ in our coordinate transformation to satisfy (3.10) and (B 6). Most importantly, $f_0(t)$ and $f_1(t)$ remain bounded because γ is a fixed separation point; as a result, all terms in the $\dot{q}$ equation remain bounded for all times.

We define the cone

$$Q = \{(q, y) \mid |q| \leqslant \alpha y, \quad 0 \leqslant y \leqslant \beta\}, \tag{D 3}$$

where α and β are positive constants to be selected below (figure 23). By our boundedness assumption on the velocity field, we can select a large enough constant $K > 0$ such that

$$|m_i(q, y, f_k, t)| \leqslant K, \qquad (q, y) \in Q, \quad t \in \mathbb{R}. \tag{D 4}$$

Consider now the $y = \beta$ boundary of the cone Q. Along this boundary, we have

$$\begin{aligned} \dot{y}|_{y=\beta} &= \beta^2 \left[c(t) + \beta m_4(q, \beta, f_k, t) + q m_5(q, \beta, f_k, t)\right] \\ &\geqslant \beta^2 \left[c(t) - K\left(\beta + \beta\alpha\right)\right] > 0, \end{aligned} \tag{D 5}$$

provided that

$$c(t) > K\beta(\alpha + 1), \tag{D 6}$$

or, equivalently,

$$v_{yy}(\gamma, 0, t) > 2K\beta(\alpha + 1). \tag{D 7}$$

Therefore, solutions intersecting the $y = \beta$ boundary of Q leave Q immediately if the inequality (D 7) holds for all times (figure 24).

Next, we consider the $q = \alpha y$ boundary of the cone Q, where we have

$$\left.\begin{aligned} \dot{q}|_{q=\alpha y} &= y^2 \alpha a_x(t) + m_1(q, y, f_k, t) y^3 + m_2(q, y, f_k, t) y^3 \alpha^2 + m_3(q, y, f_k, t) y^3 \alpha \\ &\leqslant \beta^2 [\alpha a_x(t) + K\beta(1 + \alpha^2 + \alpha)] < 0, \\ \dot{y}|_{q=\alpha y} &= y^2 [c(t) + y m_4(q, y, f_k, t) + \alpha y m_5(q, y, f_k, t)] \\ &\geqslant y^2 [c(t) - K\beta(\alpha + 1)] > 0, \end{aligned}\right\} \tag{D 8}$$

provided that

$$a_x(t) < -\frac{K\beta\left(\alpha^2 + \alpha + 1\right)}{\alpha}, \qquad c(t) > K\beta\left(\alpha + 1\right), \tag{D 9}$$

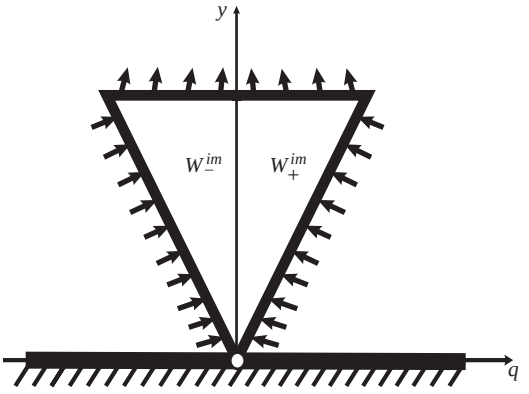

FIGURE 24. Fluid particles entering and leaving the cone Q, and the two sets W_+^{im} and W_-^{im}.

or, equivalently,

$$u_{xy}(\gamma, 0, t) < -K\beta\left(\alpha + 1 + \frac{1}{\alpha}\right), \qquad v_{yy}(\gamma, 0, t) > 2K\beta(\alpha + 1). \tag{D 10}$$

Both (D 7) and (D 10) hold if we have

$$u_{xy}(\gamma, 0, t) < -\max\left(2K\beta(\alpha + 1), K\beta\left(\alpha + 1 + \frac{1}{\alpha}\right)\right), \tag{D 11}$$

where we used the fact that $u_{xy}(\gamma, 0, t) \equiv -v_{yy}(\gamma, 0, t)$ by incompressibility. By condition (5.2), we can satisfy this last inequality by choosing the α and β parameters of the cone Q so that

$$\max\left(2\beta(\alpha + 1), \beta\left(\alpha + 1 + \frac{1}{\alpha}\right)\right) < \frac{c_0}{K}. \tag{D 12}$$

A possible choice is

$$\alpha = 1, \qquad \beta = \frac{c_0}{5K}, \tag{D 13}$$

for which we conclude that solutions intersecting the $q = \alpha$ boundary of the cone Q enter Q immediately by the estimates (D 8) (cf. figure 24). An identical argument establishes the same conclusion for the $q = -\alpha y$ boundary of Q.

Based on the above observations, we conclude that under conditions (D 7) and (D 10), the extended equations of particle motion

$$\left.\begin{aligned} \dot{q} &= yqa_x(t) + m_1(q, y, f_k, t)y^3 + m_2(q, y, f_k, t)yq^2 + m_3(q, y, f_k, t)y^2q, \\ \dot{y} &= y^2\left[c(t) + ym_4(q, y, f_k, t) + qm_5(q, y, f_k, t)\right], \\ \dot{t} &= 1, \end{aligned}\right\} \tag{D 14}$$

have the following properties on the closed set $\mathcal{Q} = Q \times \mathbb{R}$:

(*a*) The set of initial particle positions (q_0, y_0, t_0) that immediately leave $\mathcal{Q}$ in backward time is given by $W^{im} = \{(q, y, t) \in \mathcal{Q} \mid \ y > 0, \ |q| = \alpha y\}$. This is a set with two connected components

$$W_\pm^{im} = \{(q, y, t) \in \mathcal{Q} \mid \ y > 0, \ q = \pm\alpha y\}. \tag{D 15}$$

We show these sets in figure 24.

(*b*) If W^{ev} denotes the set of initial conditions (q_0, y_0, t_0) that eventually leave $\mathcal{Q}$ in backward time, then W^{im} is a relatively closed subset of W^{ev}. (This is because a sequence within $W^{im}_{\pm}$ converges to a point outside $W^{im}_{\pm}$, then that point is necessarily at $q = y = 0$, which is not in W^{ev}. Therefore, all Cauchy sequences in $W^{im}_{\pm}$ that converge to a point in W^{ev} necessarily have their limit points in $W^{im}_{\pm}$. By definition, this means that W^{im} is relatively closed in W^{ev}.)

These two properties, by definition, make $\mathcal{Q}$ a backward-time *Wasewsky set* for the extended system (D 14) (cf. Hale 1980). As a result, the Wasewsky principle holds for $\mathcal{Q}$: the map $\Gamma: W^{ev} \to W^{im}$ that maps initial positions in $\mathcal{Q}$ to the point where they leave $\mathcal{Q}$ in backward time, is continuous.

Assume now that all initial conditions with $y_0 \neq 0$ eventually leave $\mathcal{Q}$ in backward time. This would imply that

$$W^{ev} = \{(q, y, t) \in \mathcal{Q} \mid \ y > 0\}\,. \tag{D 16}$$

However, this is a contradiction, because the set W^{ev} defined above is connected, and hence cannot be mapped by a continuous map Γ into the disconnected set W^{im}. We therefore conclude that $W^{ev} \neq Q$, i.e. there is a non-empty set of initial fluid particle positions W^{∞} that stay in Q for all backward times. By definition, W^{∞} is an invariant set and is necessarily smooth in t because it is composed of fluid trajectories that are smooth in t. Also, by the continuity of the Wasewsky map, $W^{ev} = Q - W^{\infty}$ consists of two disjoint sets of initial conditions, $\mathcal{A}$ and $\mathcal{B}$, such that

$$W^{ev} = \mathcal{A} \cup \mathcal{B}, \qquad W^{im}_{+} \subset \mathcal{A}, \qquad W^{im}_{-} \subset \mathcal{B}. \tag{D 17}$$

Next we want to argue that all solutions in W^{∞} tend to $\xi = y = 0$ in backward time. Consider a specific initial position $(\bar{q}_0, \bar{y}_0, \bar{t}_0) \in W^{\infty}$, and denote the trajectory emanating from this initial position by $(q(t), y(t), t)$. Along this trajectory, we have

$$\dot{y}(t) = y^2(t)[c(t) + y(t)m_4(q, y, f_k, t) + q(t)m_5(q, y, f_k, t)] \tag{D 18}$$

which, upon integration, gives

$$y(t) = \frac{y_0}{1 + y_0 \displaystyle\int_t^{t_0} [c(\tau) + y(\tau)m_4(q, y, f_k, \tau) + q(\tau)m_5(q, y, f_k, \tau)]\,\mathrm{d}\tau}. \tag{D 19}$$

This equation holds for all $t \leqslant t_0$, because the trajectory we consider stays in $\mathcal{Q}$ for all backward times. Then (D 19) and (D 13) lead to the estimate

$$\begin{aligned} y(t) &\leqslant \frac{\beta}{1 + y_0 \displaystyle\int_t^{t_0} [c(\tau) - K\beta(\alpha + 1)]\,\mathrm{d}\tau} = \frac{\beta}{1 + y_0 \displaystyle\int_t^{t_0} \left[\frac{1}{2}v_{yy}(\gamma, 0, \tau) - K\beta(\alpha + 1)\right]\mathrm{d}\tau} \\ &\leqslant \frac{\beta}{1 + y_0 \displaystyle\int_t^{t_0} \left[\frac{1}{2}c_0 - K\beta(\alpha + 1)\right]\mathrm{d}\tau} = \frac{2\beta}{2 + y_0(c_0/5)(t_0 - t)}, \end{aligned} \tag{D 20}$$

allowing us to conclude that

$$\lim_{t \to -\infty} y(t) = 0. \tag{D 21}$$

In other words, trajectories that never leave Q in backward time will necessarily converge to the $y = 0$ boundary of the cone Q. By the definition of Q, however, this

convergence in the y-direction implies

$$\lim_{t\to-\infty} q(t) = 0. \tag{D 22}$$

We therefore conclude that all trajectories in W^∞ converge to $y = q = 0$ in backward time, thus W^∞ is an unstable manifold for $(\gamma, 0)$. Any material curve in this manifold admits bounded and unique y derivatives according to formulae (3.16)–(3.19), therefore the unstable manifold is unique up to terms of order $O(y^3)$.

The same argument applies when higher-order terms of the candidate separation profile (3.15) are included in the initial coordinate change (D 1), leading to a unique unstable manifold up to terms of order $O(y^n)$. Here, n is an arbitrary integer that can be as large as the degree of differentiability of the original velocity field.

Given the existence of the separation profile, we only need to argue that the separation is indeed sharp along this profile. To prove sharp separation, it is enough to establish that the y-coordinate of fluid particles in the separation profile W^∞ grows monotonically for all times as long as the particles are in a vicinity of the boundary. Note that W^∞ has been constructed as a material line whose $y \leqslant \beta$ portion is fully contained in the cone Q. For all fluid particles that lie in the separation profile as well as in the $\{0 < y \leqslant \beta\}$ neighbourhood of the boundary, (D 2) and (D 13) yield the estimate

$$\begin{aligned} \dot{y} &= y^2\,[c(t) + y m_4(q, y, f_k, t) + q m_5(q, y, f_k, t)] \\ &\geqslant y^2\left[\tfrac{1}{2}c_0 - K\beta(\alpha+1)\right] \geqslant y^2(c_0/10). \end{aligned} \tag{D 23}$$

Therefore, the y-coordinate of fluid particles in W^∞ grows monotonically in the $\{0 < y \leqslant \beta\}$ neighbourhood of the boundary, resulting in sharp separation.

Appendix E

Here we show that for general incompressible flows, (8.11) gives a sufficient condition for finite-time sharp separation close to the moving effective separation point $\gamma_{eff}(t, t_0)$. We shall show this by arguing that if $\gamma_{eff}(t, t_0)$ moves slowly enough for $t \in [t_0 - T_m(t_0), t_0]$, then any point $(\gamma, 0)$ close enough to $\gamma_{eff}(t, t_0)$ acts as a separation point in the Lagrangian frame over that time interval. From this argument, we obtain a set of points that can be considered finite-time separation points. The size of this set tends to zero as the admissible time scale $T_m(t_0)$ increases. As a result, in numerical calculations we obtain a separation point that is unique for practical purposes.

We start by selecting a boundary point $(\gamma, 0)$ and introducing a time-dependent coordinate change

$$q = x - \gamma - y\phi(t), \tag{E 1}$$

with $\phi(t)$ to be defined below. We obtain the transformed velocity field

$$\left.\begin{aligned} \dot{q} &= \dot{x} - \dot{y}\phi - y\dot{\phi} \\ &= y(a - \dot{\phi}) + yqa_x + y^2[(a_x - c)\phi + a_y] \\ &\quad + (l_1 y^3 + l_2 y^2 q + l_3 y q^2)(l_4 + n_1\phi), \\ \dot{y} &= y^2 C(\gamma + y\phi, y, t) \\ &= y^2[c(t) + (l_5 y + l_6 q)(l_7 + n_2\phi)], \end{aligned}\right\} \tag{E 2}$$

with appropriate smooth functions $l_j(q, y, \phi, t)$ and $n_k(q, y, \phi, t)$. These functions are typically not globally bounded in ϕ, thus they will grow unbounded if ϕ grows unbounded in time.

If we select $\phi(t)$ to satisfy

$$\dot{\phi} = a, \tag{E 3}$$

then the $O(y)$ term in the $\dot{q}$ equation of (E 2) vanishes. By our assumptions, the $O(yq)$ term remains bounded regardless of the choice of ϕ. If γ were a fixed separation point, then the solution $\phi(t)$ of (E 3) would remain bounded for all times, and hence the $O(y^3, y^2q, yq^2)$ terms in the $\dot{q}$ equation would also remain bounded for all times. However, γ is not a fixed separation point in our current setting, and hence the $O(y^3, y^2q, yq^2)$ terms in the $\dot{q}$ equation will typically grow unbounded in time.

To control the above-mentioned growth of nonlinear terms in (E 2), we select

$$\gamma = \gamma_{\mathit{eff}}(t, t_0) + \Delta(t, t_0), \tag{E 4}$$

with $\gamma_{\mathit{eff}}(t, t_0)$ denoting an effective separation point. In that case, by the mean-value theorem, any solution of (E 3) can be written as

$$\begin{aligned}\phi(t) &= \phi(t_0) + \int_{t_0}^{t} A(\gamma, 0, \tau)\,\mathrm{d}\tau = \phi(t_0) + \int_{t_0}^{t} A(\gamma_{\mathit{eff}}(t, t_0) + \Delta(t, t_0), 0, \tau)\,\mathrm{d}\tau \\ &= \phi(t_0) + \int_{t_0}^{t} \left[A(\gamma_{\mathit{eff}}(t, t_0), 0, \tau) + A_x(\gamma^*(\tau), 0, \tau)\Delta(t, t_0)\right]\mathrm{d}\tau \\ &= \phi(t_0) + \Delta(t, t_0)\int_{t_0}^{t} u_{xy}(\gamma^*(\tau), 0, \tau)\,\mathrm{d}\tau,\end{aligned} \tag{E 5}$$

for some $\gamma^*(\tau)$ falling between γ and $\gamma_{\mathit{eff}}(t, t_0)$.

Let $I(t, t_0)$ denote the maximal x interval covered by the moving effective separation point $\gamma_{\mathit{eff}}(s, t_0)$ while s varies over the time interval $[t, t_0]$. We denote the length of $I(t, t_0)$ by $\delta(t, t_0)$. If we select γ as in (8.10), then for any $t < t_0$, we have the estimate

$$\begin{aligned}|\phi(t)| &= \left|\phi(t_0) + \Delta(t, t_0)\int_{t_0}^{t} u_{xy}(\gamma^*(\tau), 0, \tau)\,\mathrm{d}\tau\right| \\ &\leqslant |\phi(t_0)| + \delta(t, t_0)\left|\int_{t_0}^{t} u_{xy}(\gamma^*(\tau), 0, \tau)\,\mathrm{d}\tau\right| \\ &\leqslant |\phi(t_0)| + \delta(t, t_0)\int_{t}^{t_0} \max_{x\in I(t,t_0)} |u_{xy}(x, 0, \tau)|\mathrm{d}\tau.\end{aligned} \tag{E 6}$$

As in Appendix D, we now define the cone

$$Q = \{(q, y)\,|\ |q| \leqslant \alpha y, \quad 0 \leqslant y \leqslant \beta\}, \tag{E 7}$$

where α and β are positive constants to be selected below. Modifying the functions l_j and $n_k\phi$ in (E 2) smoothly outside a time interval $[t_0 - T_m, t_0]$ with T_m to be determined below, we can select a constant $K > 0$ such that the modified functions satisfy

$$|l_j(q, y, \phi, t)|\,,\ \ |n_k(q, y, \phi, t)\phi| \leqslant K, \qquad (q, y) \in Q, \quad t \in \mathbb{R}. \tag{E 8}$$

Along the $y = \beta$ boundary, we now have

$$\begin{aligned}\dot{y}|_{y=\beta} &= \beta^2[c(t) + (l_5 y + l_6 q)(l_7 + n_2\phi)] \\ &\geqslant \beta^2[c(t) - 2K^2(\beta + \beta\alpha)] > 0,\end{aligned} \tag{E 9}$$

provided that

$$c(t) > 2K^2\beta(1 + \alpha), \tag{E 10}$$

or, equivalently,

$$v_{yy}(\gamma, 0, t) > 4K^2\beta(1+\alpha). \tag{E 11}$$

Therefore, solutions intersecting the $y = \beta$ boundary of Q leave Q immediately if the inequality (E 11) holds for all times.

Next we consider the $q = \alpha y$ boundary of the cone Q, where we have

$$\left.\begin{aligned} \dot{q}|_{q=\alpha y} &= y^2[\alpha a_x(t) + (a_x - c)\phi + a_y + y(l_1 + l_2\alpha + l_3\alpha^2)(l_4 + n_1\phi)] < 0, \\ \dot{y}|_{q=\alpha y} &= y^2[c(t) + y(l_5 + l_6\alpha)(l_7 + n_2\phi)] > 0, \end{aligned}\right\} \tag{E 12}$$

provided that

$$\left.\begin{aligned} \alpha a_x(t) + (a_x - c)\phi + a_y < -2K^2\beta(1+\alpha+\alpha^2), \\ c(t) > 2K^2\beta(1+\alpha). \end{aligned}\right\} \tag{E 13}$$

For fixed $\alpha > 0$, we can always select an appropriately small $\beta > 0$ such that both of these inequalities hold, provided that

$$\left.\begin{aligned} \alpha a_x(t) + \tfrac{3}{2}|a_x(t)|\left[|\phi(t_0)| + \delta(t, t_0)\int_t^{t_0} \max_{x\in I(t,t_0)} |u_{xy}(x, 0, \tau)|\,\mathrm{d}\tau\right] + |a_y(t)| < 0, \\ c(t) > 0, \end{aligned}\right\} \tag{E 14}$$

where we used the incompressibility relation $a_x + 2c = 0$.

The conditions in (E 14) hold if we require

$$\begin{aligned} \delta(t, t_0)\int_t^{t_0} \max_{x\in I(t,t_0)} |u_{xy}(x, 0, \tau)|\,\mathrm{d}\tau < \tfrac{2}{3}\left[\alpha - \max_{x\in I(t,t_0)} \frac{|u_{yy}(x, 0, t)|}{2|u_{xy}(x, 0, t)|}\right] - |\phi(t_0)|, \\ \max_{x\in I(t,t_0)} u_{xy}(x, 0, t) < 0, \end{aligned} \tag{E 15}$$

Recall that α denotes the tangent of the half-angle of the cone Q, and $\phi(t_0)$ denotes the tangent of the angle at which Q is tilted relative to the vertical in the original (x, y) coordinate system.

Our selection of the parameters α and $\phi(t_0)$ will depend on the given problem. Ideally, $\phi(t_0)$ should be chosen as the tangent of a mean value of the separation angle, and α should be chosen as the tangent of the maximal deviation of the separation angle from its mean value. To obtain a universal estimate, we select

$$\alpha = 3 + \max_{x\in I(t,t_0)} \frac{|u_{yy}(x, 0, t)|}{2\,|u_{xy}(x, 0, t)|} + \tfrac{3}{2}\,|\phi(t_0)|\,, \tag{E 16}$$

which will still accommodate sizable variations in the separation angle. (For specific problems, more refined choices of α may be possible.) For the above choice of α, the conditions (E 15) are equivalent to (8.11). Under these conditions, solutions intersecting the $q = \alpha$ boundary of the cone Q enter the cone immediately by the estimates (D 8).

With this last conclusion, the rest of our argument is identical to that of Appendix D. Following that argument, we find that γ is a fixed sharp separation point for the modified system that admits all the uniform bounds that we have assumed. As a result, the original unmodified system also admits sharp finite-time separation at γ as long as it agrees with the modified system. The resulting separation profile, however, is non-unique, which is a common feature of finite-time separation points. As a result, the choice (E 16) will give a separation profile, but not necessarily the one that ejects particles the most intensely. In particular problems, we may improve upon this conservative choice of parameters by picking a different α in (E 16).

REFERENCES

Arnold, V. I. 1978 *Ordinary Differential Equations*. MIT Press.

Cassel, K. W., Smith, F. T. & Walker, J. D. A. 1996 The onset of instability in unsteady boundary-layer separation. *J. Fluid Mech.* **315**, 223–256.

Cowley, S. J. 1983 Computer extension and analytic continuation of Blasius' expansion for impulsive flow past a circular cylinder. *J. Fluid. Mech.* **135**, 389–405.

Cowley, S. J., Van Dommelen, L. L. & Lam, S. T. 1990 On the use of Lagrangian variables in the description of unsteady boundary-layer separation. *Phil. Trans. R. Soc. Lond.* A **333**, 348–378.

Degani, A. T., Walker, J. D. A. & Smith, F. T. 1998 Unsteady separation past moving surfaces. *J. Fluid. Mech.* **375**, 1–38.

Friedlander, S. & Vishik, M. M. 1991 Instability criteria for the flow of an inviscid incompressible fluid. *Phys. Rev. Lett.* **66**, 2204–2206.

Ghosh, S., Leonard, A. & Wiggins, S. 1998 Diffusion of a passive scalar from a no-slip boundary into a two-dimensional chaotic advection field. *J. Fluid Mech.* **372**, 119–163.

Grunberg, O., Surana, A. & Haller, G. 2004 Three-dimensional unsteady separation: a kinematic theory. Preprint.

Hackborn, W. W., Ulucakli, M. E. & Yuster, T. 1997 A theoretical and experimental study of hyperbolic and degenerate mixing regions in chaotic Stokes flow. *J. Fluid Mech.* **346**, 23–48.

Hale, J. K. 1980 *Ordinary Differential Equations*. Krieger, Malabar, FL.

Haller, G. & Poje, A. 1998 Finite-time transport in aperiodic flows. *Physica* D **119**, 352–380.

Haller, G. 2000 Finding finite-time invariant manifolds in two-dimensional velocity fields. *Chaos* **10**, 99–108.

Haller, G. 2001 Lagrangian structures and the rate of strain in two-dimensional turbulence. *Phys. Fluids* A **13**, 3365–3385.

Lifshitz, A. 1991 Essential spectrum and local stability conditions in hydrodynamics. *Phys. Lett.* A **152**, 199–204.

Lighthill, M. J. 1963 Boundary layer theory. In *Laminar Boundary Layers* (ed. L. Rosenhead). Dover.

Liu, C. S. & Wan, Y.-H. 1985 A simple exact solution of the Prandtl boundary layer equations containing a point of separation, *Arch. Rat. Mech. Anal.* **89**, 177–185.

Lugt, H. 1995 *Vortex Flow in Nature and Technology*. Krieger, Malabar, FL.

Moore, F. K. 1958 On the separation of unsteady boundary layer. In *Boundary-layer Research* (ed. H. Görtler) pp. 296–311. Springer.

Peridier, V. J. 1995 A Lagrangian scheme for the animation of unsteady separation. *Computers Fluids* **24**, 269–291.

Perry, A. E. & Chong, M. S. 1986 A series expansion study of the Navier–Stokes equations with applications to three-dimensional separation patterns. *J. Fluid Mech.* **173**, 207–223.

Prandtl, L. 1904 Über Flüssigkeitsbewegung bei sehr kleiner Reibung. *Verh. III, Int. Math. Kongr., Heidelberg* pp. 484–491.

Rott, N. 1956 Unsteady viscous flows in the vicinity of a separation point. *Q. Appl. Maths* **13**, 444–451.

Schlichting, H. & Gersten, K. 2000 *Boundary Layer Theory* (8th edn) Springer.

Sears, W. R. & Tellionis, D. P. 1971 Unsteady boundary layer separation. In *Recent Research on Unsteady Boundary Layers* (ed. E. Eichelbrenner), pp. 404–447.

Sears, W. R. & Tellionis, D. P. 1975 Boundary-layer separation in unsteady flow. *SIAM J. Appl. Maths* **28** 215–235.

Shariff, K., Pulliam, T. H. & Ottino, J. M. 1991 A dynamical systems analysis of kinematics in the time-periodic wake of a circular cylinder. *Lect. Appl. Math.* **28**, 613–646.

Sobey, I. J. 2000 *Introduction to Interactive Boundary Layer Theory*. Oxford University Press.

Tritton, D. J. 1988 *Physical Fluid Dynamics*. Oxford University Press.

Van Dommelen, L. L. 1981 *Unsteady Boundary Layer Separation*. PhD thesis, Cornell University, Ithaca, NY.

Van Dommelen, L. L. & Cowley, S. J. 1990 On the Lagrangian description of unsteady boundary layer separation. Part 1. General theory. *J. Fluid Mech.* **210**, 593–626.

Van Dommelen, L. L. & Shen, S. F. 1982 The genesis of separation. In *Numerical and Physical Aspects of Aerodynamics Flow* (ed. T. Cebici) pp. 283–311. Long Beach, California.

Wang, Y., Haller, G., Banaszuk, A. & Tadmor, G. 2003 Closed-loop Lagrangian separation control in a bluff body shear flow model. *Phys. Fluids* A **15**, 2251–2266.

Williams, J. C. 1977 Incompressible boundary layer separation. *Annu. Rev. Fluid. Mech.* **9**, 113–144.

Wu, J. Z., Tramel, R. W., Zhu, F. L. & Yin, X. Y. 2000 A vorticity dynamics theory of three-dimensional flow separation. *Phys. Fluids* A **12**, 1932–1954.

Yuster, T. & Hackborn, W. W. 1997 On invariant manifolds attached to oscillating boundaries of Stokes flows. *Chaos* **7**, 769–776.